



Optimal designs with topology optimisation

Master thesis report

A. B. L. Frank

Optimal designs with topology optimisation

by

A.B.L. FRANK

Master thesis report
to obtain the degree of Master of Science
at the Delft University of Technology,
to be defended publicly on May 18, 2022 at 14:00.

Abstract: The level-set approach in the field of topology optimisation has been studied thoroughly the last two decennia, but there is a lack of challenging standard benchmark problems. Besides two standard benchmark problems, this master's thesis tackles one difficult benchmark problem in particular: the inverter. For every benchmark the minimum compliance problem is solved numerically. A level-set based algorithm has been devised to detect if a structure has a discontinuity during the optimisation process. In addition to this, a prevention method is tested, yet the results are unsatisfactory.

Keywords: Topology optimisation, level-set method, minimum compliance, connectivity.

Student number: 4603443

Project duration: July 26, 2021 – May 18, 2022

Thesis committee

Daily supervisor university

Dr. ir. D. den Ouden-van der Horst Delft University of Technology

Responsible professor

Prof. dr. ir. C.Vuik Delft University of Technology

Daily supervisor company

Dr. J. Pereira Machado Sioux Technologies

Committee member

Prof. ir. H.M. Schuttelaars Delft University of Technology

This thesis report is confidential and cannot be made public until May 10, 2022

An electronic version of this thesis is available at [//repository.tudelft.nl/](https://repository.tudelft.nl/).

PREFACE

As announced in my literature report, the purpose of this preface is to thank some people. If the reader is interested in the outline of this report, I suggest reading the preface of the corresponding literature report. However, I would simply recommend reading this final report. I promise that it will be a good read.

First, I would like to thank all my colleagues at Sioux Mathware, where I conducted my research. I learned a lot from them and enjoyed the time I spend there in Eindhoven. In particular, I want to thank my company supervisor João, with whom I had countless meetings to discuss important and unimportant matters. Obrigado João!

Second, I would like to thank my family and friends. I suppose my friends know that they are my friends, so I do not deem it necessary to mention them all. My wonderful parents, however, have to be mentioned. They have always supported me during my educational career.

Third, I urge Richard to hurry up with his master thesis. Also I would like to thank him for the moral support. During our weekly conversations at the dinner table we could talk about the frustrations and difficulties of graduating. Moreover, I wish him all the best with his master thesis.

Last but not least, I would like to thank all the teacher of the Applied Mathematics and Education department. I had a fantastic time as a student at Delft University of Technology.

Of course, I must not forget my amazing daily supervisor, whom I know since my first year in Delft. During my time at the university Dennis and I worked a lot together, and although I learned a great deal from him, I never had him as a teacher ironically. Dennis, ontzettend bedankt!

*Abel Frank
Bilthoven, May 2022*

CONTENTS

Preface	iii
1 Introduction	1
1.1 Field of interest	1
1.2 Historical background	2
1.3 Research problem	4
1.4 Thesis objectives	4
1.5 The reader's guide to the thesis	5
2 Preliminaries	7
2.1 The physical design	7
2.1.1 Material properties	7
2.1.2 Physical constraints	8
2.2 Mathematical domain	8
2.2.1 Reference domain	8
2.2.2 Material domain	9
2.2.3 Boundary conditions on Γ	10
2.2.4 Place-dependency of parameters and constants	10
3 Benchmark problems	11
3.1 Comparative topology optimisation method	11
3.2 MBB beam	12
3.2.1 Numerical examples MBB beam	13
3.3 Cantilever	15
3.3.1 Numerical example cantilever	16
3.4 Inverter	19
3.4.1 Numerical example inverter	20
4 Derivation of the minimum compliance problem	25
4.1 Linear elasticity	25
4.1.1 Stiffness tensor	26
4.2 The principle of minimum potential energy	27
4.3 Minimum compliance problem	28

4.4	The level-set method	29
4.4.1	Properties of the level-set function	30
4.5	Implementing the level-set method	31
4.5.1	Level-set embedded minimum compliance problem	32
5	Solving the minimum compliance problem	33
5.1	KKT conditions	33
5.2	Update procedure	34
5.2.1	Reaction-diffusion equation	35
5.2.2	Topological derivative	36
5.3	Discretisation	37
5.3.1	In time	37
5.3.2	In space	38
5.3.3	Bounded level-set function	40
5.3.4	Volume constraint	41
5.3.5	Algorithm	42
5.4	Numerical results	42
5.4.1	MBB beam	43
5.4.2	Cantilever	45
5.4.3	Inverter	48
6	Connectivity	51
6.1	Path connectedness	51
6.2	Detection algorithm	52
6.2.1	Detection loop	52
6.2.2	False positive	53
6.2.3	Problems with m_b elements	56
6.2.4	Two diagonal internally connected elements	58
6.2.5	Final detection algorithm	59
6.3	Prevention	60
6.4	Combining detection and prevention	61
6.5	Results of the new algorithm	63
6.5.1	Alternative prevention algorithm	63
7	Conclusion and discussion	67
7.1	Conclusion	67
7.2	Discussion	68
A	Derivation of the equation of motion	71
B	Nomenclature	73

CHAPTER 1

INTRODUCTION

1.1 Field of interest

Structures (e.g. bridges, beams and hinges) with optimal designs are becoming more significant in our society in which efficiency and sustainability are vital. Obtaining the most efficient design for complex structures is a delicate task of colossal (industrial) importance. Optimal designs lead to better performances and lighter structures and save design materials. A drawback of optimal designs is that they may be expensive or difficult to manufacture. Traditional design methods primarily deal with straightforward and basic geometries. This obviously puts a restriction on the complexity of the structures one might want to design and optimise.

Nowadays, fortunately, there are methods which do not have this problem. Three commonly used methods are size, shape and topology optimisation. While size and shape optimisation methods require close-to-optimal initial designs, topology optimisation does not. In topology optimisation (TO) an objective function is minimised (or maximised) under physical and geometrical constraints with the material distribution as a problem variable. In other words, the aim of topology optimisation is to find the optimal design under an objective and adhering a number of constraints.

A major part of this thesis focuses on a well-known topology optimisation problem, namely the minimum compliance problem. The objective is to find a design for which the compliance is minimal under a number of constraints. In the context of linear elasticity the compliance is equivalent to the strain energy. This energy dictates the stiffness of a structure in the following way: if the strain energy is minimal, the stiffness of the design is maximal. Choosing this objective results in the strongest structure.

Although topology optimisation yields many advantages in comparison to older methods, solving the affiliated minimum compliance problem poses some obstacles. Finding analytical solutions turns out to be a tedious task and in most cases they do not exist. Even solving the minimum compliance problem numerically presents us with specific issues. Three common numerical problems are the formation of checkerboards, mesh dependency and local minima, which, amongst others, will be discussed in Sec-

tion 1.2.

In light of checkerboard formation and mesh dependency, level-set methods (LSM) have been proposed to circumvent them. Moreover, level-set based topology optimisation methods yield a beneficial treatment of changes in the topology during the optimisation process. In level-set methods, the design or material domain is represented implicitly by a level-set function (LSF), of which the zero interface describes the boundary of this domain.

In addition to level-set based topology optimisation, the connectivity of the final design is of significant importance too. From a mechanical point of view a manufacturer wants certain parts of the structure to be connected to each other. Two problems regarding connectivity are the formation of the aforementioned checkerboards and the formation of disconnected parts of the final design.

1.2 Historical background

In the year 1988 two very important mathematical papers were published. The topic of each paper plays a major role in this thesis. Bendsøe and Kikuchi [8] are the founding fathers of topology optimisation and Sethian and Osher [24] the architects of the level-set method.

In 1988 Bendsøe and Kikuchi introduced a method that generates optimal topologies utilising the homogenisation method (for more information on the homogenisation method for topology optimisation, see [1] and [39]). In their paper the foundation for topology optimisation was laid. Since then, numerous topology optimisation approaches have been developed. The basis of these approaches, however, is the same and gives answer to the fundamental question of topology optimisation: where to place material in a prescribed domain for the best structural performance?

For a broader review of the field of topology optimisation see the 2014 survey of Deaton and Grandhi [12]. For a comparison of the different topology optimisation methods see the comparative review of Sigmund and Maute [35].

A branch of topology optimisation that does not get a lot of attention, but is worth exploring, is the subject of connectivity. One of the most straightforward connectivity constraints is avoiding the formation of enclosed voids in the design structure and is used in various manufacturing processes. For example, this constraint is applied in additive manufacturing (commonly known as 3D printing), see the 2021 book of Gibson et al. [15] for more information on the subject of additive manufacturing. In the context of level-set topology optimisation Kasaiezadeh and Khajepour wrote an article [16] in 2011 on how to use the level-set function to avoid discontinuity in the structure.

Naturally, problems occur when solving a topology optimisation problem. The 0-1 topology optimisation problem, for example, lacks analytical solutions in general [36], [35]. However, there are some cases for which an analytical solution is found [17], [18], [19], [27], [28]. Furthermore, there are numerical problems. In their 1998 review article [36] Sigmund and Petersson indicate three common numerical problems which occur in topology optimisation. First, there is the formation of checkerboards. This is the construction of alternating void and solid elements ordered in a checkerboard pattern caused by the non-convergence of finite-element solutions. Second, we have mesh

dependency. This refers to the problem that for different mesh-sizes or discretisations one does not obtain qualitatively the same solution. Third, there is the existence of local minima. This means that for the same discretisation one obtains different solutions if algorithmic parameters are altered, e.g., different initial designs. This is caused by the numerical optimisation procedures of the optimisation algorithm.

Since 1988 a number of different approaches has been developed as Sigmund and Maute point out in their review article [35]. These include density, level-set, topological derivative, phase field and evolutionary approaches. A thorough comparison of these different approaches and other literature reference can be found in the same review article.

As this thesis focuses on the level-set approach, it is important to understand what the level-set method is. In 1988 Sethian and Osher published a paper about capturing fronts propagating with curvature-dependent speed [24]. Later it was named the level-set method and is thoroughly described in the book of Osher and Fedkiw [23]. This method describes how one keeps track of a level-set (in most cases the zero level contour) of a function. This function is called the level-set function and the contour is also referred to as the interface, as it separates positive and negative regions. In 2000 the level-set method was applied in topology optimisation for the first time by Sethian and Wiegmann [31]. Since then, various level-set based topology optimisation methods have arisen. These can be classified, for example, by the approach for updating the level-set field in the optimisation process and the method for discretising the level-set function. In their review article Van Dijk et al. pay attention to these different approaches and discuss the level-set approach in general [42].

The level-set method for topology optimisation was introduced because of the special properties of the level-set function. The function is used to implicitly define the interfaces between materials by iso-contours. This allows for a neat description of the interfaces. Some notable works in the field of level-set topology optimisation are that of Noël et al. [21] who use hierarchical B-splines to discretise the state variable fields and level-set function, Yaji et al. [45] who embed the reinitialisation of the level-set function in the time evolution equation utilising a convected level-set method and Allaire and Jouve [3] who adapt the method for stress minimisation.

The reason we choose a level-set based topology optimisation over other approaches, is because it holds many advantages and it is a relatively new approach. The main advantage is that the interface is clearly and smoothly described implicitly by the level-set function. In addition, Allaire et al. state a number of benefits for the level-set approach in their 2004 paper [5]. The method permits radical topological changes during the optimisation process, the CPU time is reasonable and it can handle general mechanical models (including nonlinear ones) and objective functionals. In the aforementioned comparative review paper of Sigmund and Maute [35] the level-set approach is also reviewed. They remark that the level-set method is “well suited for capturing stochastic shape variations for robust design optimization”. In the review article of Van Dijk et al. [42] it is also noted that a level-set based topology optimisation algorithm treats topological changes conveniently, unlike explicit boundary description methods. This means that during the optimisation process holes can fuse together and new connections can be made in the design.

Unfortunately, there are drawbacks to a level-set approach for topology optimisation. A huge deficiency in the conventional level-set approach was that it did not

allow the nucleation of holes. This is noted by Allaire et al. ([2], [5], [6]) and techniques to circumvent this are briefly outlined. This lack of hole nucleation makes the optimal design heavily dependent on the initial design as stated in plentiful works (Allaire et al. [5], Sigmund and Maute [35], Van Dijk et al. [42] and Yaji et al. [45]). Furthermore, similar to the traditional topology optimisation method, the level-set based method suffers from local minima according to Allaire and Jouve [2] and Van Dijk et al. [42]. Luckily, the majority of these obstacles has been dealt with. However, there is also a non-numerical problem in topology optimisation. This will be part of the research problem and is discussed in the next section.

1.3 Research problem

The use of standard benchmark problems for topology optimisation methods is briefly addressed in the 2013 comparative review article of Sigmund and Maute [35]. While the MBB beam and cantilever are typical benchmark problems in literature, there is a lack of challenging standard test cases. Moreover, they mention a specifically “challenging but still simple to implement compliant mechanism benchmark”: the inverter. It was first proposed by Sigmund in 1997 [32] and used as a ‘standard’ benchmark problem in later works of him and co-writers [33], [34]. In Section 3.4 the inverter benchmark problem will be thoroughly described.

Sigmund and Maute recommend in their review article that the inverter example should be chosen as a standard benchmark problem in future works regarding topology optimisation and in particular level-set based topology optimisation. The heavy influence of the initial design is a substantial burden for boundary control methods (e.g. level-set methods).

Another problem the author wishes to take on is the lack of an algorithm which can detect discontinuities in the design structure during the optimisation process and prevent those from occurring. While Kasaiezadeh and Khajepour [16] detect a discontinuity based on the physics, an algorithm which actually looks at the material distribution has not been proposed yet.

1.4 Thesis objectives

The first step of this thesis is to find out how a level-set embedded minimum compliance problem can be solved numerically. This means developing a topology optimisation algorithm based on the level-set method that is able to interact with a finite-element model and using it to find optimal designs. In view of this we set the following objectives:

- Derive a level-set embedded minimum compliance problem.
- Solve this problem numerically, which leads to an algorithm.
- Compare the results of this algorithm to known benchmarks: MBB beam, cantilever and inverter.

At the hand of these objectives we want to contribute to the solution for standardised benchmark problems.

Once these objectives have been accomplished, we move on to the connectivity problem for which we set the following objectives:

- Formulate an algorithm which can detect a discontinuity during each step of the optimisation process based on the material distribution derived from the level-set function.
- Expand the detection algorithm such that it can prevent the final design from having discontinuities.
- Implement the prevention algorithm into the algorithm which solves the level-set embedded minimum compliance problem.

1.5 The reader's guide to the thesis

Now that a background of the main topic has been presented and the research problem of the thesis along with its corresponding objectives has been established, a concise overview of the outline of this literature report is provided below.

Chapter 2 (Preliminaries)

Essential physical and material constraints as well as clarifying mathematical notations are treated in this chapter.

Chapter 3 (Benchmark problems)

Three benchmark problems regarding the minimum compliance problem are introduced and discussed thoroughly. Besides this, a comparative topology optimisation method is briefly addressed and used to show some results of these benchmarks.

Chapter 4 (Minimum compliance problem derivation)

Some elemental definitions of linear elasticity along with the principle of minimum potential energy are introduced at first. The main topic of this chapter is the derivation and formulation of the minimum compliance problem.

Chapter 5 (Solving the minimum compliance problem)

Different methods and approaches for solving the minimum compliance problem numerically are discussed. One approach is applied and results are examined.

Chapter 6 (Connectivity)

The matter of connectivity is utterly studied. First, an algorithm to detect a discontinuity is devised and improved. Second, a prevention constraint is introduced. Finally, detection and prevention are combined into an algorithm and tested for the minimum compliance problem.

Chapter 7 (Conclusion and discussion)

In this final chapter conclusions are drawn, discussions are conducted and the thesis is brought to an end.

CHAPTER 2

PRELIMINARIES

The physical and mathematical framework in which the problems of this thesis are presented is treated in this chapter. It begins with the physical aspects of the design material. Finally, those aspects are translated into a mathematical model.

2.1 The physical design

First and foremost, it must be noted that all physical designs are three-dimensional. However, as will be stated later, the mathematical problem can be two-dimensional as well. This is due to the fact that two-dimensional mathematical shapes can be constructed as three-dimensional, physical structures. In engineering this procedure is known as extrusion.

To start off, it is important to specify the properties we want our material to have.

2.1.1 Material properties

The material that will be used for the design is isotropic and homogeneous. A material is said to be isotropic if its properties are the same in all directions. Homogeneous means that a material has the same properties everywhere in the domain.

Throughout this thesis steel is used as the design material. In Table 2.1 the parameter values of steel are displayed. These values are used in all codes and benchmark test cases.

Notation	Definition	Value in SI units
ρ	Density	$7.750 \text{ kg} \cdot \text{m}^{-3}$
E	Young's modulus	$190 \cdot 10^9 \text{ Pa}$
ν	Poisson ratio	0.28

Table 2.1: *Table of the parameter values of steel.*

2.1.2 Physical constraints

Naturally, the design does have a number of physical constraints. One of the most important constraints we pose on the design is a volume limit. This limit is defined as V_{\max} and is a volume fraction. That is, it denotes a fraction of the total volume available to construct the design.

Essential elements of designing are design constraints. These constraints can be translated into physical constraints. The physical constraints treated in this thesis consist of two material constraints and two mechanical constraints. The material constraints dictate in which regions material must be present and in which no material is allowed.

The first mechanical constraint relates to the boundary conditions and the second states that the design structure must be connected, which will be thoroughly treated in Chapter 6. For now, there is not explicit constraint on the connectivity of the material domain. In the next section the constraints are explained in more detail and expressed in mathematical terms.

2.2 Mathematical domain

It is imperative to define the mathematical domain in which we work. This can be either \mathbb{R}^2 or \mathbb{R}^3 in the case of topology optimisation. For the sake of generality, however, we shall refer to \mathbb{R}^d where d is the dimension of the space. The domain we focus on is defined as the *reference domain* Ω . This domain is a subset of the whole domain, i.e., $\Omega \subseteq \mathbb{R}^d$. We refer to the design material/structure as the *material domain* and assign it the letter D . This material domain is always ‘inside’ the reference domain, i.e., $D \subseteq \Omega$. The boundary of the material domain, ∂D , is denoted by Γ . All space within the reference domain that is not material is called the void. It should be pointed out that the use of D and Ω is typical in papers concerning topology optimisation. It differs per paper which notation is used for the reference domain and which for the material domain (also called design domain).

To make a clear distinction between a volume integral (area integral in \mathbb{R}^2) and a surface integral (line integral in \mathbb{R}^2) we also use the capital Greek letters omega and gamma to denote these integrals, respectively. So, a volume integral has the differential $d\Omega$ and a surface integral $d\Gamma$.

Promptly, more specific information about the reference and material domain is given.

2.2.1 Reference domain

The reference domain can have any fixed form. So, it does not necessarily need to be a square (or cube) or circle (or sphere). Due to this definition of the reference domain, we give the material domain a predefined space in which we want it to be optimised. It also puts a limit on the available space for the material domain. That is to say, the aforementioned volume fraction V_{\max} is a fraction of the volume of the reference domain. A pleasant fortuity is that we can create holes, which serve as regions where no material is allowed, in the reference domain. Furthermore, the boundary of the reference domain, $\partial\Omega$, is significant too, as it is needed to define the boundary conditions of the level-set function. This, however, will be accounted for after the level-set

method is introduced and implemented into the minimum compliance problem (see Section 4.5).

2.2.2 Material domain

The objective of topology optimisation is to find the optimal design. Therefore, we must be clear on what the material domain D is. It is crucial to keep in mind that the material domain will be updated during the optimisation process. This means that we start with an initial material distribution, i.e., the initial design. Finally, we end up with an optimal material distribution, i.e., the final and optimal design.

The material domain D is the set of coordinates where material is present. It is contained in the reference domain and cannot exist outside of it. Due to possible design constraints we allow the initial material domain to have predefined holes. Moreover, it is even possible that new holes are created as a consequence of the topology optimisation. We must also take into account that there may be parts of the material domain where material must be present. Therefore we define the domain $A \subseteq D$. That is, A is the subset of D where there is always material. A simple visualisation of all this is given in Figure 2.1. Although we will not encounter any benchmark problems which have a set A in the interior of D , it is important to define A in this way in order to stay generic. In our benchmark problems A is part of the boundary of D .

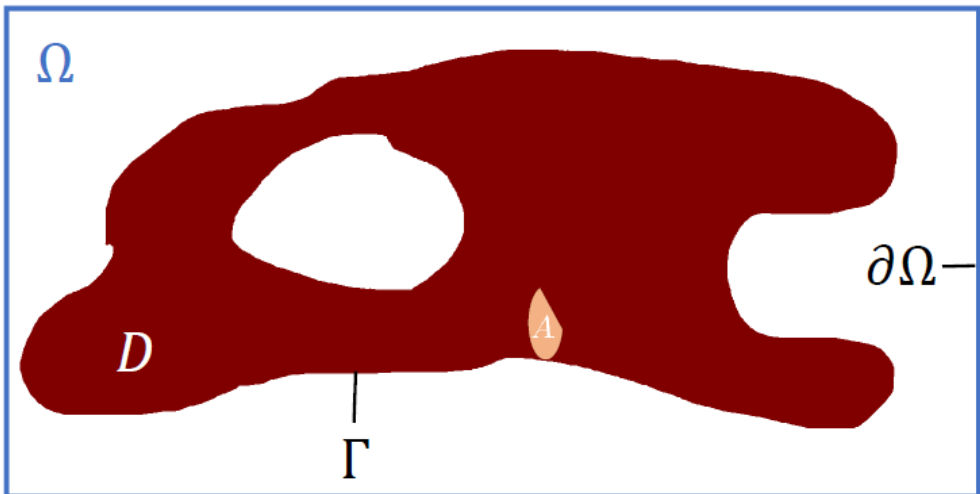


Figure 2.1: *Two-dimensional visualisation of the mathematical domain. Ω is the reference domain and $\partial\Omega$ its boundary. The material domain is D and Γ its boundary. Material is always present in A .*

2.2.3 Boundary conditions on Γ

In this thesis only two types of boundary conditions are considered: Dirichlet boundary conditions (named after Peter Gustav Lejeune Dirichlet) and Neumann boundary conditions (named after Carl Neumann). Therefore, we define Γ_D , the part of the boundary which has Dirichlet boundary conditions, and Γ_N , the part which has Neumann boundary conditions, such that $\Gamma = \Gamma_D \cup \Gamma_N$. These boundary conditions apply to the displacement \mathbf{u} (which is explained in Chapter 4). Moreover, some parts of the boundary can have both boundary conditions. However, a single displacement component (u_x , u_y or u_z) can only have one boundary condition.

We have two types of mechanical conditions on Γ which result in boundary conditions:

1. An external force \mathbf{t} on the boundary. This gives a Neumann boundary condition at the point where the force is exerted. So, there has to be material present at this point.
2. Fixed material on the boundary. This gives a Dirichlet boundary condition, i.e., $\mathbf{u} = \mathbf{0}$. Obviously there is material present on this part of the boundary.

If no explicit boundary condition is stated for a certain part of the boundary it is assumed to have a homogeneous Neumann boundary condition.

It should be pointed out that often the boundary of D partly coincides with the boundary of Ω . This happens at places where either one of the aforementioned mechanical boundary conditions are defined.

2.2.4 Place-dependency of parameters and constants

Because we make a clear difference between material and void, the parameters and constants we encounter are place-dependent in a certain way. Inside the material domain, i.e., in the material, the parameters and constants exist. As the material is isotropic and homogeneous the parameters and constants remain the same everywhere inside the material domain. On the other hand, in the void, those parameters and constants do not exist. So, the parameters and constants could be expressed with the use of an indicator function, but that would only be necessary in computational cases. Thus, we will refrain from denoting parameters and constants as functions of place.

In the next chapter this mathematical framework is translated into concrete examples.

CHAPTER 3

BENCHMARK PROBLEMS

This chapter examines three benchmarks which will later be used to test the level-set based topology optimisation algorithm for the minimum compliance problem, which is derived in the subsequent chapter. To provide a frame of reference, a comparative algorithm is used to solve these benchmarks as well. To be clear, this chapter does not contain the level-set approach. We start this chapter with a brief description of this comparative algorithm.

3.1 Comparative topology optimisation method

Before we discuss the comparative topology optimisation method, we first take a look at a simplified version of the minimum compliance problem:

$$\begin{cases} \min_{\rho} & f(\rho) \\ \text{s.t.} & \int_{\Omega} \rho \, d\Omega \leq V_{\max} \int_{\Omega} d\Omega, \\ & \rho(\mathbf{x}) = \mathbb{1}_{\mathbf{x} \in D}. \end{cases} \quad (3.1)$$

Here f is the objective function, which in our case is the compliance, and the second line is the volume constraint. The last line in Problem (3.1) shows that the density is equal to 1 inside the material domain and 0 outside of it. This means that the optimisation variable is discrete: a 0-1 topology optimisation problem. Due to the discrete nature of Problem (3.1) it is generally hard to solve according to Sigmund and Petersson [36]. Approximation the discrete problem with continuous design variables proves to be easier. A method which does this, is the density approach known as SIMP (Simple Isotropic Material with Penalisation). Also called the power-law approach, the SIMP approach considers the design variables to be continuous (i.e. $0 \leq \rho(\mathbf{x}) \leq 1$) and forces these towards a black and white solution with the use of a penalisation parameter. This means that intermediate densities (also called grey transition areas)

are allowed, but pushed to either 0 or 1. The best choice for this penalisation parameter p turns out to be $p = 3$ [35]. For more information on SIMP see [9], [35] and [36]. The well-known finite-element method (FEM) is used for the discretisation and utilises rectangular elements. Moreover, a Helmholtz filter prevents the formation of checkerboard patterns. This filter ensures that the material has a minimum thickness, has the problem of generating grey transition areas between void and solid elements. We use a filter radius of $r_{\min} = \frac{0.75 \cdot \text{width}}{\#\text{horizontal elements}}$. The iterative updating is done by the method of moving asymptotes (MMA) (Svanberg [40]). The volume constraint is $V_{\max} = 0.5$ and the maximum number of iterations is $n_{\max} = 200$. The stopping criteria are the following two: the relative change of the objective function is below 10^{-2} and the infinity norm of the solution is below 10^{-2} .

3.2 MBB beam

The Messerschmitt-Bölkow-Blohm (MBB) beam is a well-known standard benchmark problem in the field of topology optimisation (see [21] and [34]). It consists of a beam for which the bottom left and right points are fixed. So, these two points have homogeneous Dirichlet conditions in the horizontal and vertical direction. On the middle top point a force is exerted as shown in Figure 3.1. This is considered a Neumann boundary condition, as mentioned in Chapter 3.

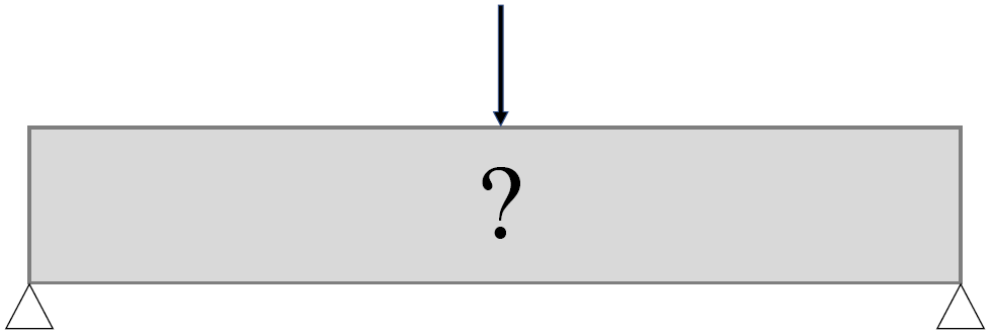


Figure 3.1: *Reference domain of the MBB beam and the boundary conditions.*

Due to symmetry, we merely have to model half of the design. As shown in Figure 3.2, the symmetric axis is the vertical line through the applied force. This leads to a mathematically induced, mechanical boundary condition: there can be no displacement in the horizontal direction on this newly created boundary. So, on the left boundary we have one homogeneous Dirichlet condition ($u_x = 0$) and two homogeneous Neumann conditions ($u_{y,x} = u_{z,x} = 0$). The reason we do this, is to create a smaller reference domain which is computationally more efficient. The rest of the boundary, except the bottom right point, has a homogeneous Neumann condition. For results in other literature see the 2007 paper of Sigmund [33] and the 2010 paper of Takewaza et al. [41] (the latter refers to it as a bridge).

For our MBB beam benchmark problem we consider a width to height ratio of 6:1

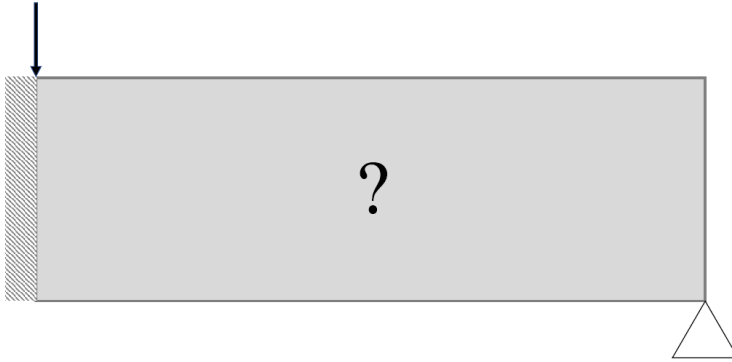


Figure 3.2: *Reference domain of the right-hand side of the MBB beam and the boundary conditions.*

(entire beam). Regarding the physical dimensions, our entire MBB beam has a width of 0.6 m and height of 0.1 m.

3.2.1 Numerical examples MBB beam

For these numerical examples we look at MBB beams with 24 by 8 (Figure 3.4), 48 by 16 (Figure 3.5) and 96 by 32 (Figure 3.6) elements in horizontal and vertical direction respectively. In Figure 3.3 we see the initial material density distribution of the 48 by 16 MBB beam. The presence of material in the bottom right and top left corners is clearly visible. The former represents the fixed point and the latter is the point where the downward force is exerted.

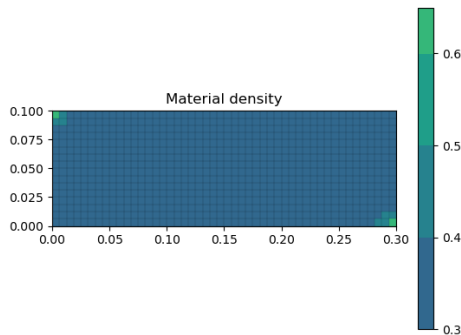


Figure 3.3: *Initial material density distribution of the 48 by 16 MBB beam with the SIMP approach.*

From Figure 3.4a it is not quite clear that it is the MBB beam compared to results in literature. The figure solely indicates that the structure goes from the top left corner to the bottom right corner. This gives reason for a higher resolution. Remarkable is that the structure did converge in 130 iterations. Figure 3.4b indicates that the convergence was monotonic.

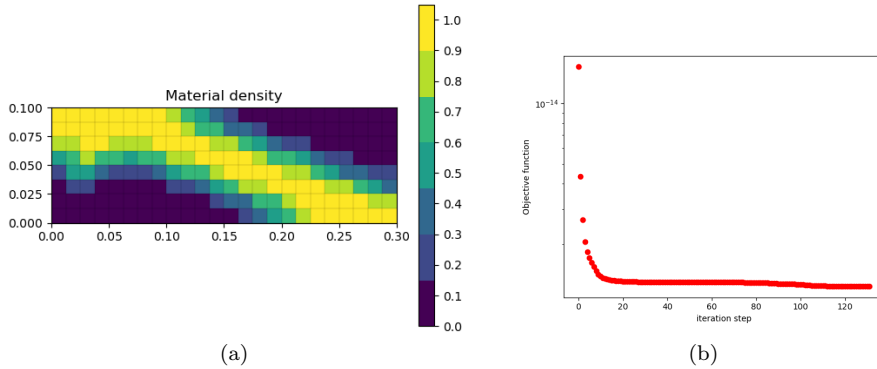


Figure 3.4: *Final design 24 by 8 MBB beam with SIMP approach: (a) material density distribution; (b) Evolution of the objective function.*

If we double the number of horizontal and vertical elements the final design (Figure 3.5a) becomes much clearer, as expected. We can now see that a new part has been constructed in the lower left corner. This was not yet visible in the final design with a lower resolution (see Figure 3.4a). If we take a look at the convergence plot in Figure 3.5b, we see that convergence is quicker (97 iterations). In addition to this, the objective function is also monotonically decreasing.

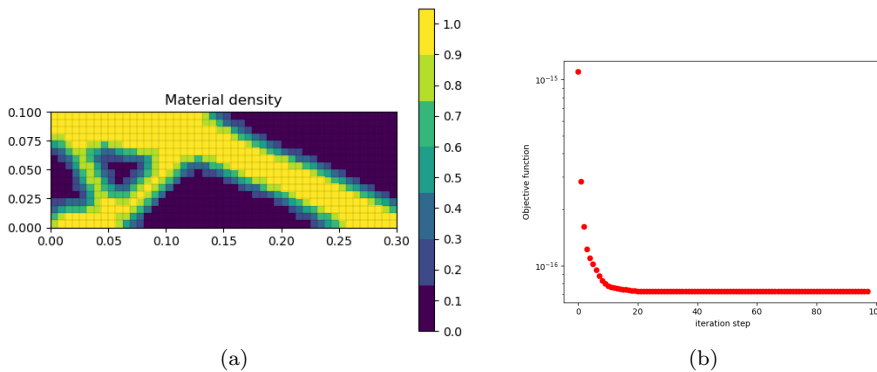


Figure 3.5: *Final design 48 by 16 MBB beam with SIMP approach: (a) material density distribution; (b) Evolution of the objective function.*

Figure 3.6a clearly shows a form of convergence in the final design of the MBB beam. The structure looks the same as the 48 by 16 MBB beam (see Figure 3.5a), but has a higher resolution and the boundary is sharper and more distinct. This is a result of the higher number of elements (96 by 32). Remarkable is the fact that it took 196 iterations to converge, as is shown in Figure 3.6b. We would expect it to take less iterations than the other two configurations, because it has a finer mesh. It turns out that the convergence criterion for the objective function was satisfied after 22 iterations, but it took significantly more iterations to obey the criterion on the

infinity norm of the solution. The objective function seems to decrease monotonically, but after 25 iterations it looks to have converged completely.

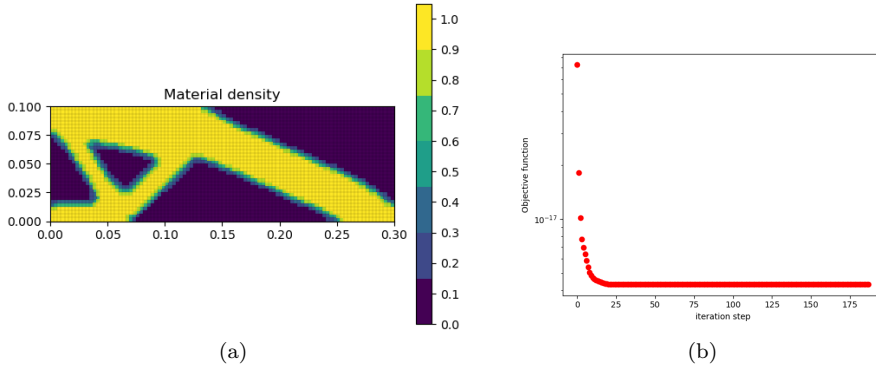


Figure 3.6: *Final design 96 by 32 MBB beam with SIMP approach: (a) material density distribution; (b) Evolution of the objective function.*

It is clear that the results of the 24 by 8 MBB beam are not useful for industrial purposes in comparison to the higher resolution results. The 48 by 16 MBB beam showed clear signs of convergence in the final design. The boundary, nonetheless, was not clear and a higher resolutions is required if one desires to manufacture this structure. The best results were, as could be expected, provided by the structure with the highest resolution. The convergence to the optimal final design is evident and the boundary of the structure is distinguishable as well. A serious drawback we observed in Figure 3.6b was the a vast amount of iterations needed to converge which takes a lot of CPU time. This problem can be circumvented by abandoning the criterion on the infinity norm of the solution. A higher number of elements seems undue, but could be necessary for additive manufacturing machines.

3.3 Cantilever

If one benchmark problem is required to be present, then it must be the cantilever benchmark problem. In all fields of topology optimisation the cantilever problem is commonplace, as it is simple to implement and solve. Some examples of the cantilever in literature are found in [4], [39] and [41].

The cantilever is a rectangle of which the left edge is fixed (as if to a wall). So, we have homogeneous Dirichlet conditions on the entire left-hand side of the rectangle. Furthermore, there is a concentrated force vertically loaded at the centre point of the right-hand side (see Figure 3.7). The rest of the boundary of the rectangle has homogeneous Neumann conditions. We examine a cantilever with a 2:1 width to height ratio. Regarding the physical dimensions, our cantilever has a width of 0.2 m and height of 0.1 m.

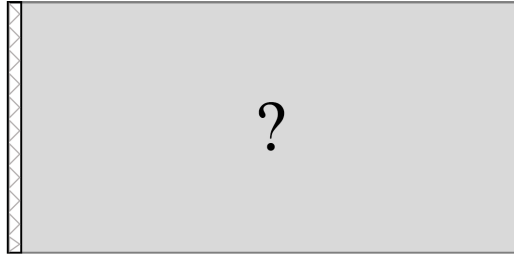


Figure 3.7: *Reference domain of the cantilever and the boundary conditions.*

3.3.1 Numerical example cantilever

For these numerical examples we look at cantilevers with 16 by 8 (Figure 3.9), 32 by 16 (Figure 3.10) and 64 by 32 (Figure 3.11) elements. In Figure 3.8 the initial material density distribution of the cantilever is depicted. The material constraint of predefined material at the left-hand side is visible in the initial design. The entire left edge consists of material is fixed. On the right hand side are two elements with material upon which force is exerted. The reason that this are two elements, is because the code used for the comparative algorithm can only place material in an element and not around or on a node. With two elements the the average force is still in the middle of the right edge.

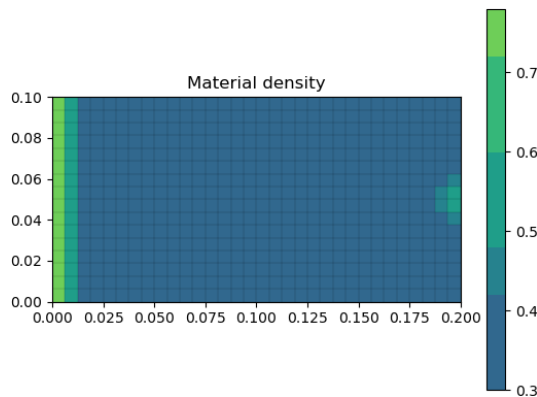


Figure 3.8: *Initial material density distribution of the 32 by 16 cantilever with the SIMP approach.*

The final design of the 16 by 8 cantilever depicted in Figure 3.9a does not tell us much about what the structure is and where its boundary is. Only a clear hole in the middle of the left-hand side has formed. Furthermore, there are a lot of elements which have a density of 0.5. So, it is not clear whether or not there is material in those elements. Figure 3.9b indicates that the objective function decreases monotonically, but did not reach the convergence criteria within 200 iterations.

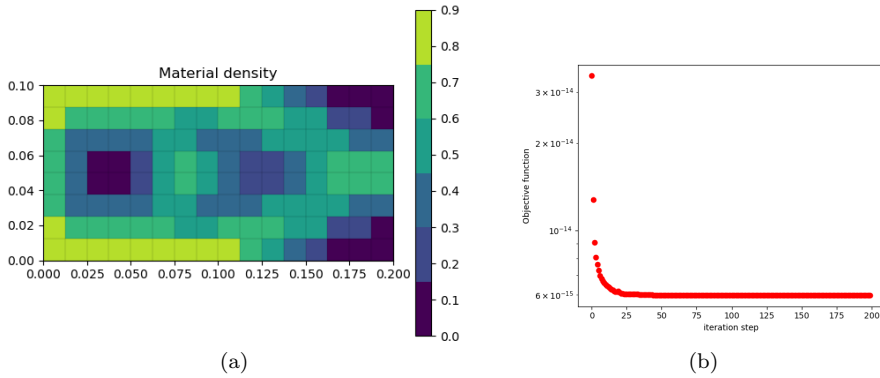


Figure 3.9: *Final design 16 by 8 cantilever with SIMP approach: (a) material density distribution; (b) Evolution of the objective function.*

Figure 3.10a shows a clearer structure than the previous configuration. Four holes have emerged; two big ones and two smaller ones. The boundary still is not very distinct. Similar to the 16 by 8 cantilever the 32 by 16 cantilever has a monotonically decreasing objective function (see Figure 3.10b). The convergence criteria, however, are again not reached.

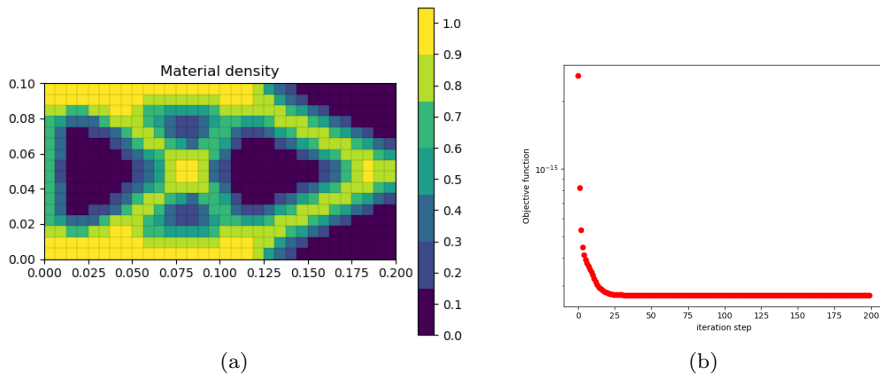


Figure 3.10: *Final design 32 by 16 cantilever with SIMP approach: (a) material density distribution; (b) Evolution of the objective function.*

The best result is achieved with the highest resolution as we can see in Figure 3.11a. Moreover, we see a form of convergence in the structure itself. The 64 by 32 cantilever has the same outlines as the 32 by 16 cantilever, except that it has a more distinct boundary and better resolution. This is a consequence of the higher number of elements. A huge difference with the previous two configurations is that the final design converged in 154 iterations. This can be seen in Figure 3.11b. It is important to point out that the criterion on the objective function was reached after 67 iterations. To reach the criterion on the infinity norm of the solution took another

87 iterations.

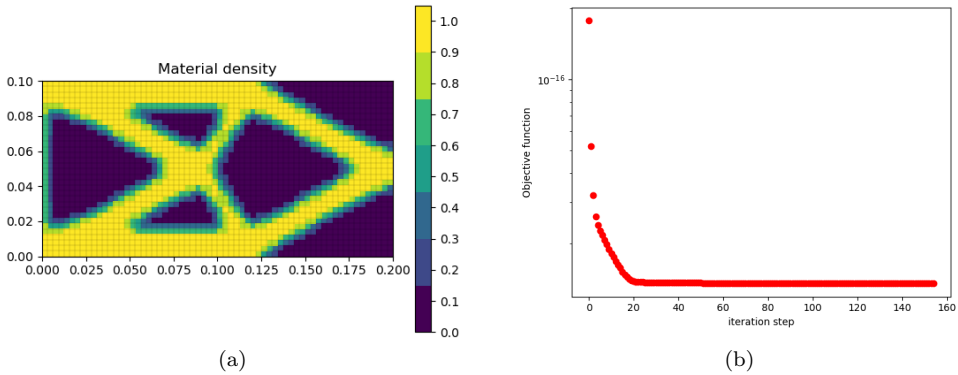


Figure 3.11: *Final design 64 by 32 cantilever with SIMP approach: (a) material density distribution; (b) Evolution of the objective function.*

It should be pointed out that the results above heavily depend on the Helmholtz filter. If we were to lower the filter radius, we would have more holes and finer features. This is visualised in Figure 3.12, where we used a filter radius of $r_{\min} = 2.34375 \cdot 10^{-4}$ as opposed to a filter radius of $r_{\min} = 2.34375 \cdot 10^{-3}$ in Figure 3.11a. The reason for this is because the cantilever has an analytic solution with an infinite amount of infinitely thin fibers (Lewiński[18]). Now, if we would not apply a density filter and use the Optimality Criteria (OC) method for the update procedure, we see in Figure 3.13 that checkerboards are formed. Also, in the boundary regions there are barely any grey transitions between void and material elements. We used OC instead of MMA, because the latter requires a density filter.

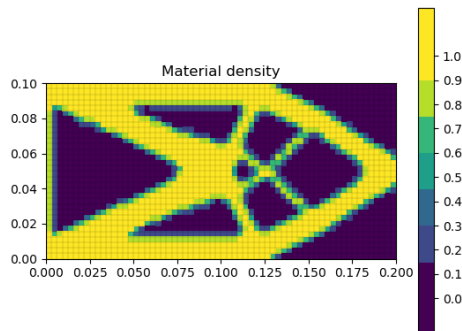


Figure 3.12: *Final design 64 by 32 cantilever with SIMP approach and lower filter radius ($r_{\min} \approx 2.3 \cdot 10^{-4}$).*

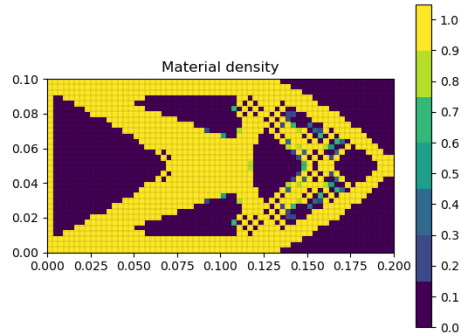


Figure 3.13: *Checkerboard formation in the final design of the 64 by 32 cantilever. SIMP approach with OC and no density filter.*

3.4 Inverter

The inverter is to a certain extent different from the MBB beam and cantilever. While the first two benchmark problems have the objective of minimising the compliance, in the inverter problem the objective is to minimise the displacement in a certain point in one direction. On account of this, the inverter problem will be dismissed as a compliant mechanism problem and treated as a minimum compliance problem. A compliant mechanism problem would mean a second problem, besides the minimum compliance problem. Which would be outside the scope of this thesis. Nonetheless, a short description of the original inverter problem will be provided. The inverter

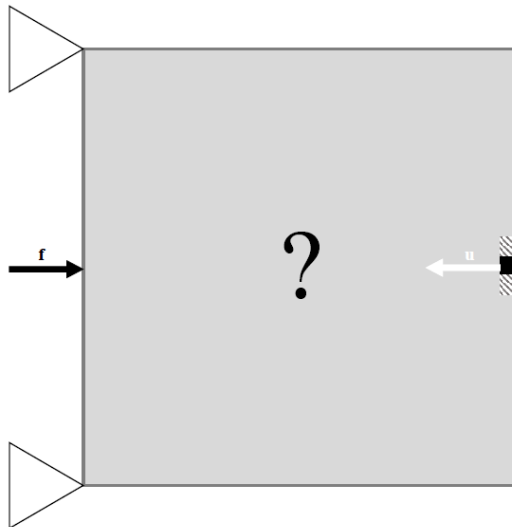


Figure 3.14: *Reference domain of the inverter and the boundary conditions.*

is a “force or displacement-inverting mechanism and is used to change the direction

of actuating displacement or force” according to Veguería et al. [43]. The reference domain is a square where the left-hand side top and bottom corners are fixed (homogeneous Dirichlet). A force is exerted on the middle of the left edge in the horizontal direction. This force can point to the left of or to the right. On the right-hand side in the middle of the square there is a point which can only be displaced in the horizontal direction (see Figure 3.14). So, we have a homogeneous Dirichlet condition for the vertical component of this point.

Like the MBB beam, the inverter also has a symmetry property which is illustrated in Figure 3.15.

In the setting of minimum compliance we do not alter the physical model of the inverter. The difference is the objective, which is now finding the optimal design wherefore the compliance is minimal.

Regarding the physical dimensions, our square inverter has a width of 0.2 m and height of 0.2 m.

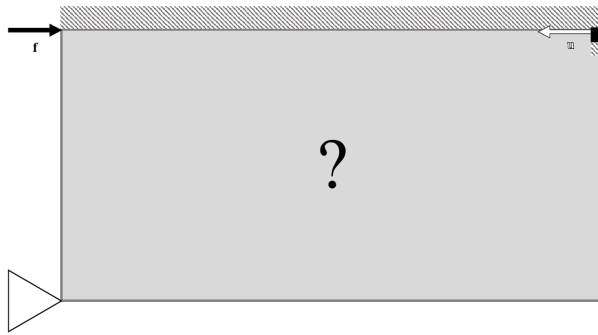


Figure 3.15: *Reference domain of the lower side of the inverter and the boundary conditions.*

3.4.1 Numerical example inverter

For these numerical examples we look at inverters with 16 by 8 (Figure 3.17), 32 by 16 (Figure 3.18) and 64 by 32 (Figure 3.19) elements. Figure 3.16 shows the initial material density distribution of the inverter. The material constraint of predefined material at the bottom left and top right corners is visible in the initial design.

Figure 3.17 immediately shows us an interesting anomaly: the final design has a discontinuity. The point in the top right corner is not connect to the rest of the structure. If we look at the two other plots with higher resolution (Figure 3.18a and Figure 3.19a), we see that this discontinuity is not due to the lower number of elements of the 16 by 8 inverter. The only difference we can now distinguish, is a space of void on the left-hand side. As anticipated and seen in the two other benchmarks, a higher number of elements results in a clearer structure with a distinct boundary.

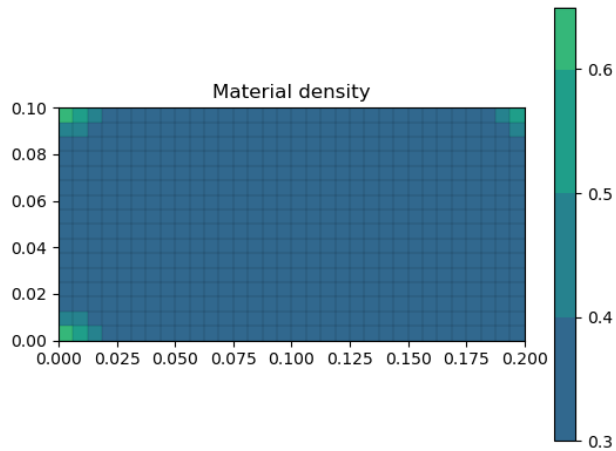


Figure 3.16: *Initial material density distribution of the 32 by 16 cantilever with the SIMP approach.*

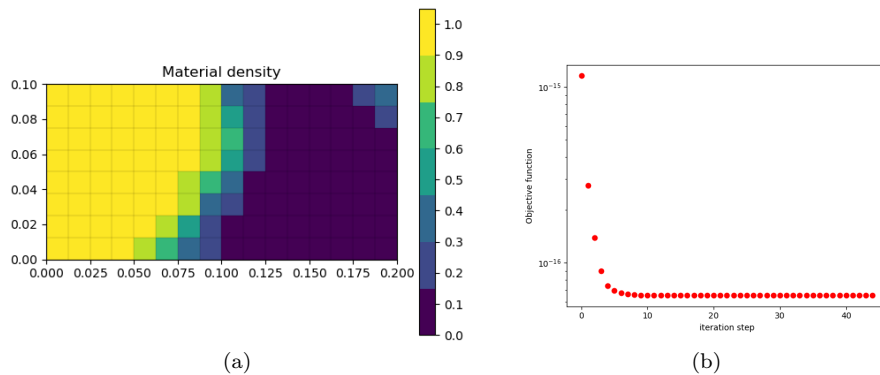


Figure 3.17: *Final design 16 by 8 MBB beam with SIMP approach: (a) material density distribution; (b) Evolution of the objective function.*

If we look at the convergence plot of all resolutions (Figures 3.17b, 3.18b and 3.19b in ascending order of total number of elements), we can conclude that the algorithm has converged. Moreover, the total number of iterations for all configurations is around 45. So, the number of elements has no influence on the rate of convergence.

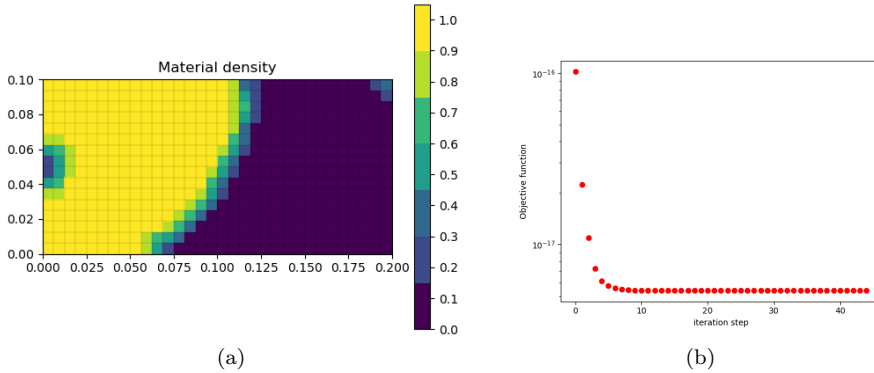


Figure 3.18: *Final design 32 by 16 inverter with SIMP approach: (a) material density distribution; (b) Evolution of the objective function.*

This discontinuity is undesirable and allows for further investigation. We want to know when this discontinuity occurs. So, we test another number of elements and look at different stages of the iteration process.

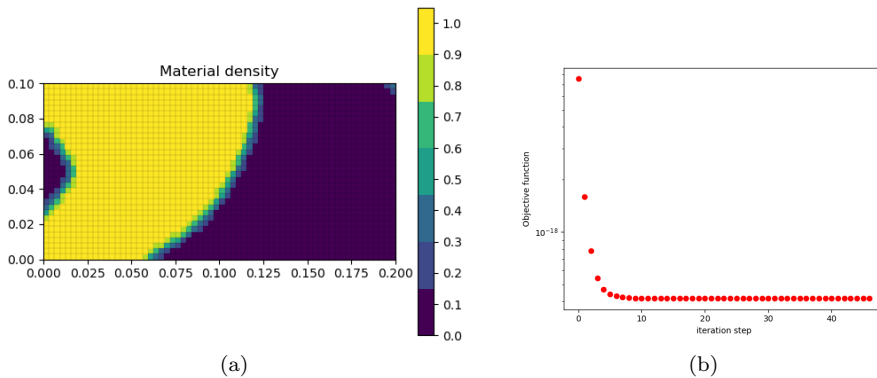


Figure 3.19: *Final design 64 by 32 inverter with SIMP approach: (a) material density distribution; (b) Evolution of the objective function.*

In Figure 3.20 we see four iteration steps of the 50 by 25 inverter. After 24 iterations we must conclude that the design is not as we intent it to be; connected. A void is created between the top right point and the rest of the structure if we compare the initial design (Figure 6.9a) to the design after 1 iteration (Figure 6.9b). After the second iteration (Figure 6.9c, the two points on the left-hand side tend to connect. This could be due to the strong local minimum Sigmund and Maute mention in their review article [35]. It is, however, more likely that this is simply the optimal design, as the used algorithm does not guarantee ‘connectedness’. This gives an incentive to figure out if a level-set approach deals with this connectivity issue.

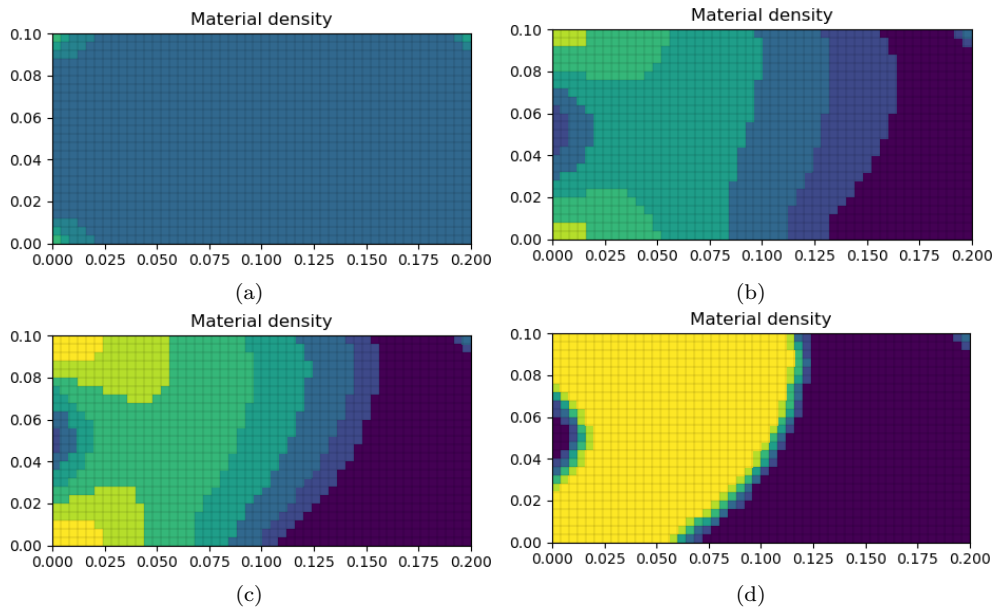


Figure 3.20: *Iteration steps of the 50 by 25 inverter with the SIMP approach: (a) initial design; (b) 1 iteration; (c) 2 iterations; (d) 24 iterations.*

CHAPTER 4

DERIVATION OF THE MINIMUM COMPLIANCE PROBLEM

In this chapter we compose the topology optimisation problem after a brief introduction to linear elasticity and the principle of minimum potential energy in physics. Then, the minimum compliance problem is derived. Finally, we implement the level-set method into the minimum compliance problem. First, we look at the physics of linear elasticity.

4.1 Linear elasticity

Elasticity involves a change of shape, so we define the *displacement vector* $\mathbf{u}(\mathbf{x})$ as a function of the location $\mathbf{x} \in \mathbb{R}^d$. As stated by Sadd [30] the (Cauchy) strain consists of *normal strain*, which is “the change in length per unit length of fibers oriented in the normal direction”, and *shear strain*, which is “the change in angle between two originally orthogonal directions in the continuum material”. According to Sadd [30] there is a relation between the displacement and the strain, which is called the *strain-displacement relation*

$$\underline{\underline{\varepsilon}}(\mathbf{u}) := \frac{1}{2} (\nabla \mathbf{u} + (\nabla \mathbf{u})^T), \quad \varepsilon_{ij} = \frac{1}{2} \left(\frac{\partial u_i}{\partial x_j} + \frac{\partial u_j}{\partial x_i} \right). \quad (4.1)$$

Note that $\underline{\underline{\varepsilon}}(\mathbf{u})$ is a symmetric tensor by definition, i.e., $\varepsilon = \varepsilon^T$. Be aware of the fact that the strain-displacement relation is linearised; ergo the name linear elasticity. For information regarding the theory of nonlinear elasticity see Antman’s book [7] (in the context of mathematics) or Rushchitsky’s book [29] (in the context of physics). If one is interested in nonlinear elasticity in relation to topology optimisation, the 2004 paper of Allaire et al. [5] is recommended.

Another very important physical quantity is *stress*. In order to express the stress in

terms of the strain we utilise a generalised version of Hooke's law (named after Robert Hooke) for linear, isotropic and, elastic materials [37]:

$$\underline{\underline{\varepsilon}} = \frac{1}{E} [(1 + \nu)\underline{\underline{\sigma}} - \nu \text{tr}(\underline{\underline{\sigma}})I], \quad (4.2)$$

where E is the Young's modulus, ν the Poisson ratio (named after Thomas Young and Siméon Poisson, respectively), $\underline{\underline{\sigma}}$ the stress tensor and I the identity matrix. In index notation this becomes $\varepsilon_{ij} = \frac{1}{E} [(1 + \nu)\sigma_{ij} - \nu\delta_{ij}\sigma_{kk}]$, where $\sigma_{kk} = \sum_{i=1}^d \sigma_{ii}$ and δ_{ij} is the Kronecker delta function (named after Leopold Kronecker). Remark that

$$\begin{aligned} \varepsilon_{kk} &= \frac{1}{E} [(1 + \nu)\sigma_{11} - \nu\sigma_{kk} + (1 + \nu)\sigma_{22} - \nu\sigma_{kk} + (1 + \nu)\sigma_{33} - \nu\sigma_{kk}] \\ &= \frac{1}{E} [(1 + \nu)\sigma_{kk} - 3\nu\sigma_{kk}] = \frac{1 - 2\nu}{E}\sigma_{kk}. \end{aligned}$$

This gives $\sigma_{kk} = \frac{E}{1-2\nu}\varepsilon_{kk}$. Now we can express the stress tensor in terms of the linear strain tensor.

$$\sigma_{ij} = \frac{E}{1 + \nu}\varepsilon_{ij} + \frac{\nu E}{(1 + \nu)(1 - 2\nu)}\delta_{ij}\varepsilon_{kk}.$$

If we introduce the Lamé constants, $\lambda = \frac{\nu E}{(1 + \nu)(1 - 2\nu)}$ and $\mu = \frac{E}{2(1 + \nu)}$ (named after Gabriel Lamé), we can give the constitutive equation for isotropic materials (Hooke's law) as described in [37].

$$\underline{\underline{\sigma}}(\mathbf{u}) = 2\mu\underline{\underline{\varepsilon}}(\mathbf{u}) + \lambda \text{tr}(\underline{\underline{\varepsilon}}(\mathbf{u}))I. \quad (4.3)$$

It should be mentioned that μ is also known as the *shear modulus* in the context of elasticity.

4.1.1 Stiffness tensor

As we are dealing with linear elasticity, the stress components are assumed to be linear functions of the strain components. So, following Equation (4.3), we can express the stress as

$$\sigma_{ij}(\mathbf{u}) = E_{ijkl}\varepsilon_{kl}(\mathbf{u}), \quad \text{with} \quad E_{ijkl} = \mu(\delta_{ik}\delta_{jl} + \delta_{il}\delta_{jk}) + \lambda\delta_{ij}\delta_{kl}. \quad (4.4)$$

The term E_{ijkl} is called the *stiffness tensor* and for an isotropic homogeneous material has the following symmetry properties:

$$E_{ijkl} = E_{jikl}, \quad E_{ijkl} = E_{ijlk}, \quad E_{ijkl} = E_{klij}. \quad (4.5)$$

The first two symmetries are a consequence of the symmetry of the strain in Relation (4.1). Due to the third symmetry we can define the following symmetric bilinear function in Einstein notation (named after Albert Einstein):

$$a(\mathbf{u}, \mathbf{v}) := \int_D E_{ijkl}\varepsilon_{kl}(\mathbf{u})\varepsilon_{ij}(\mathbf{v}) \, d\Omega, \quad (4.6)$$

where D is the aforementioned design domain. Definition (4.6) is loosely based on an inner product introduced by Eremeyev and Lebedev [13]. Later, we will see that

Definition (4.6) is the *energy bilinear form* as described by Bendsøe and Sigmund [9] and used in the formulation of the minimum compliance problem. Using the stiffness tensor expression of the stress (see Equation (4.4)), Definition (4.6) can be written as

$$a(\mathbf{u}, \mathbf{v}) = \int_D \underline{\underline{\sigma}}(\mathbf{u}) : \underline{\underline{\varepsilon}}(\mathbf{v}) \, d\Omega. \quad (4.7)$$

Here the Frobenius inner product (named after Ferdinand Georg Frobenius) is used. The Frobenius inner product for two complex-valued $n \times m$ matrices A and B is defined as follows:

$$A : B := \langle A, B \rangle_F = \sum_{i,j} \overline{A_{ij}} B_{ij}, \quad (4.8)$$

where the overline denotes the complex conjugate. It follows from its definition that the Frobenius inner product is sesquilinear.

4.2 The principle of minimum potential energy

From the principle of minimum potential energy we can derive the weak form of linear elasticity, which is called the *the principle of virtual work* in stress analysis. The minimum potential energy problem of an elastic body, based on [13] and [37], is defined as

$$\begin{cases} \text{Find } \mathbf{u} \in U \text{ such that } P(\mathbf{u}) \leq P(\mathbf{v}) \, \forall \mathbf{v} \in U, \text{ for} \\ P(\mathbf{u}) = \frac{1}{2} \int_D \underline{\underline{\sigma}}(\mathbf{u}) : \underline{\underline{\varepsilon}}(\mathbf{u}) \, d\Omega - \int_{\Gamma} \mathbf{t} \cdot \mathbf{u} \, d\Gamma - \int_D \mathbf{f} \cdot \mathbf{u} \, d\Omega, \end{cases} \quad (4.9)$$

where \mathbf{t} is the (external) traction, \mathbf{f} the (internal) body forces and U the set of all accessible displacements. Traction forces only act on the boundary of the design domain. Traction can be seen as the force which makes an object move over a surface by overcoming all resisting forces. In our case we regard externally applied traction forces. Body force is a force that acts on the whole design domain. Examples of body forces are gravity and (electro)magnetism.

Now, we want to find weak extrema of the functional $P(\mathbf{u})$ which denotes the *total strain energy for an elastic body*. Therefore, we look at the calculus of variations. This tells us that a necessary condition for finding weak extrema for Problem (4.9) is the *Euler-Lagrange equation* (named after Leonhard Euler and Joseph-Louis Lagrange):

$$\left. \frac{d}{d\beta} P(\mathbf{u} + \beta \mathbf{v}) \right|_{\beta=0} = 0 \quad (4.10)$$

for any fixed virtual displacement $\mathbf{v} \in U_0 := \{\mathbf{w} \in U : \mathbf{w} = \mathbf{0} \text{ on } \Gamma_D\}$ and \mathbf{u} the optimal solution of Problem (4.9). Here, U_0 denotes the set of admissible displacements with homogeneous Dirichlet boundary conditions.

Before we express the Euler-Lagrange equation, note that the functional $P(\mathbf{u})$ can be expressed in terms of the aforementioned symmetric bilinear function a , see Definition (4.6). This results in

$$P(\mathbf{u}) = \frac{1}{2} a(\mathbf{u}, \mathbf{u}) - \int_{\Gamma} \mathbf{t} \cdot \mathbf{u} \, d\Gamma - \int_D \mathbf{f} \cdot \mathbf{u} \, d\Omega.$$

Using this expression for the functional, we first look at $P(\mathbf{u} + \beta\mathbf{v})$ and express it using the symmetric and bilinear properties of $a(\mathbf{u}, \mathbf{v})$.

$$P(\mathbf{u} + \beta\mathbf{v}) = \frac{1}{2}a(\mathbf{u}, \mathbf{u}) + \beta a(\mathbf{u}, \mathbf{v}) + \frac{1}{2}\beta^2 a(\mathbf{v}, \mathbf{v}) - \int_{\Gamma} \mathbf{t} \cdot \mathbf{u} \, d\Gamma - \beta \int_{\Gamma} \mathbf{t} \cdot \mathbf{v} \, d\Gamma - \int_D \mathbf{f} \cdot \mathbf{u} \, d\Omega - \beta \int_D \mathbf{f} \cdot \mathbf{v} \, d\Omega.$$

We take the derivative with respect to β .

$$\frac{d}{d\beta} P(\mathbf{u} + \beta\mathbf{v}) = a(\mathbf{u}, \mathbf{v}) + \beta a(\mathbf{v}, \mathbf{v}) - \int_{\Gamma} \mathbf{t} \cdot \mathbf{v} \, d\Gamma - \int_D \mathbf{f} \cdot \mathbf{v} \, d\Omega.$$

Now we set $\beta = 0$ and equate the result to zero.

$$a(\mathbf{u}, \mathbf{v}) - \int_{\Gamma} \mathbf{t} \cdot \mathbf{v} \, d\Gamma - \int_D \mathbf{f} \cdot \mathbf{v} \, d\Omega = 0.$$

So, the weak form of linear elasticity is

$$\int_D \underline{\underline{\sigma}}(\mathbf{u}) : \underline{\underline{\varepsilon}}(\mathbf{v}) \, d\Omega = \int_D \mathbf{f} \cdot \mathbf{v} \, d\Omega + \int_{\Gamma} \mathbf{t} \cdot \mathbf{v} \, d\Gamma \quad \forall \mathbf{v} \in U_0. \quad (4.11)$$

From Equation (4.11) the *equation of motion for elastostatics* can be derived. For this derivation look at Appendix A.

4.3 Minimum compliance problem

As mentioned before, the functional of Definition (4.6) is used in the minimum compliance problem as the internal virtual work. The sum of integrals on the right-hand side of Equation (4.11) is called the *load linear form* [9]. We define the functional

$$l(\mathbf{u}) := \int_D \mathbf{f} \cdot \mathbf{u} \, d\Omega + \int_{\Gamma} \mathbf{t} \cdot \mathbf{u} \, d\Gamma. \quad (4.12)$$

The way we define the minimum compliance problem is roughly based on the same problem defined by Bendsoe and Sigmund in their book [9].

$$\left\{ \begin{array}{l} \min_D a(\mathbf{u}, \mathbf{u}) \\ \text{s.t. } a(\mathbf{u}, \mathbf{v}) = l(\mathbf{v}), \quad \forall \mathbf{v} \in U_0, \\ \mathbf{u}|_{\Gamma_D} = \mathbf{u}_0, \\ A \subseteq D, \\ \int_D 1 \, d\Omega \leq V_{\max} \int_{\Omega} 1 \, d\Omega. \end{array} \right. \quad (4.13)$$

Here D and Γ_D are as described in Section 2.2. The objective of the minimum compliance problem is to find the optimal design domain for which the compliance is

minimal. This is equivalent to minimising the strain energy ($\frac{1}{2}a(\mathbf{u}, \mathbf{u})$) over D . Note that this is the same as minimising $a(\mathbf{u}, \mathbf{u})$ over D , which is the objective of Problem (4.13). What is more, we minimise over D and not over \mathbf{u} , contrary to Bendsøe and Sigmund [9]. That is because \mathbf{u} is a function of the design domain D ; \mathbf{u} is determined by the principle of minimum potential energy which depends on the shape of D . Furthermore, Problem (4.13) consists of the physical constraint regarding the principle of minimum potential energy, a boundary condition and the volume constraint, in that order. The homogeneous Neumann boundary condition is processed into the weak form of linear elasticity.

Now, we aim to incorporate the level-set method into Problem (4.13). Therefore, we shortly digress for a brief introduction to the level-set method.

4.4 The level-set method

The level-set method was introduced in 1988 by Sethian and Osher [24] in order to keep track of the motion of an arbitrary interface. The method involves using a *level-set function*:

$$\begin{cases} \phi(\mathbf{x}) > 0 & \forall \mathbf{x} \in \Omega \setminus D \text{ (void),} \\ \phi(\mathbf{x}) = 0 & \forall \mathbf{x} \in \Gamma \cap \Omega \text{ (interface),} \\ \phi(\mathbf{x}) < 0 & \forall \mathbf{x} \in D \setminus \Gamma \text{ (material).} \end{cases} \quad (4.14)$$

A visualisation of this scalar function is provided by Figure 4.1. In Figure 4.1 the unit normal vector on the interface, which is introduced in the next section is visible as well.

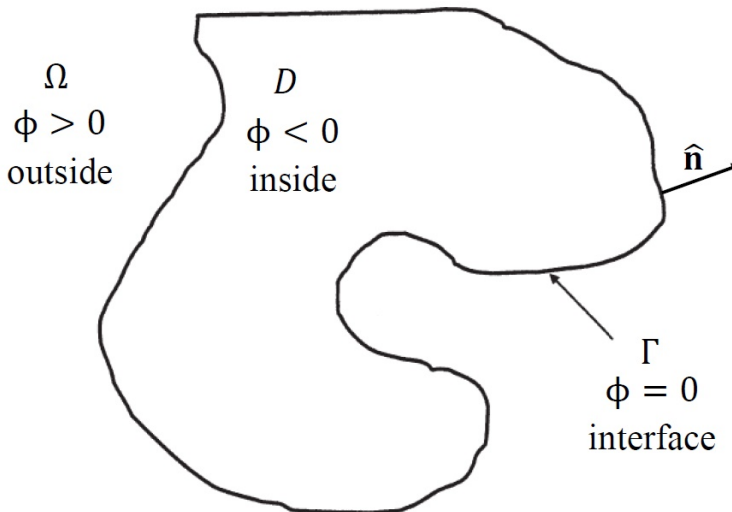


Figure 4.1: *Graphical representation of the level-set function.*

4.4.1 Properties of the level-set function

Some convenient and interesting properties follow from Definition (4.14).

Unit normal

The gradient, $\nabla\phi$, is perpendicular to the isocontours of ϕ and points in the direction of increasing ϕ (on the zero interface that is, from the material to the void). Let \mathbf{x}_0 be a point on the zero isocontour of ϕ , then $\nabla\phi(\mathbf{x}_0)$ is a vector that points in the same direction as the local unit normal vector, $\hat{\mathbf{n}}$, on that isocontour in \mathbf{x}_0 . Thus, we can express this normal vector in terms of the level-set function for points on the interface.

$$\hat{\mathbf{n}}(\mathbf{x}) = \frac{\nabla\phi(\mathbf{x})}{\|\nabla\phi(\mathbf{x})\|}. \quad (4.15)$$

Note that Equation (4.15) holds for any interface $\phi = a$ with $a \in \mathbb{R}$.

Volume and surface integrals

Using the Heaviside function, Dirac delta function and a level-set function one can compose a *volume integral* (area or length integral in \mathbb{R}^2 or \mathbb{R} , respectively) and *surface integral* (line or point integral in \mathbb{R}^2 or \mathbb{R} , respectively) over the entire reference domain Ω .

The Heaviside function (named after Oliver Heaviside) is defined as follows using the (one-dimensional) variable ϕ :

$$H(\phi) := \begin{cases} 1 & \text{if } \phi > 0, \\ 0 & \text{if } \phi \leq 0. \end{cases} \quad (4.16)$$

For convenience purposes we define the Dirac delta function (named after Paul Dirac) as the derivative of the Heaviside function

$$\delta(\phi) := H'(\phi). \quad (4.17)$$

As the level-set function is place-dependent, the volume integral of a function $f(\mathbf{x})$ over the interior D is defined as

$$\int_D f(\mathbf{x}) \, d\Omega := \int_{\Omega} f(\mathbf{x}) (1 - H(\phi(\mathbf{x}))) \, d\Omega. \quad (4.18)$$

Notice, how the integral on the right-hand side is over the entire reference domain. This an advantage if integrating over Ω is more convenient than integrating over D . Before we move on to the surface integral, we have to show some equalities. Osher and Fedkiw [23] state that the directional derivative of the Heaviside function in the normal direction is a Dirac delta function which depends on the multidimensional variable \mathbf{x} :

$$\tilde{\delta}(\mathbf{x}) := \nabla H(\phi(\mathbf{x})) \cdot \hat{\mathbf{n}}. \quad (4.19)$$

It is important to remark that this definition differs from the definition used by physicists: $\hat{\delta}(\mathbf{x}) := \delta(x_1) \cdots \delta(x_d)$.

Due to how the level-set function is defined, the function $\tilde{\delta}(\mathbf{x})$ is only non-zero on the interface Γ . With this definition of the Dirac delta function the surface integral of a function $f(\mathbf{x})$ over the boundary Γ is defined as

$$\int_{\Gamma} f(\mathbf{x}) \, d\Gamma := \int_{\Omega} f(\mathbf{x}) \tilde{\delta}(\mathbf{x}) \, d\Omega. \quad (4.20)$$

Notice how we go from a boundary integral to an integral over the entire reference domain.

In order for us to implement the level-set function into this boundary integral, we rewrite Definition (4.19) using the chain rule.

$$\begin{aligned} \tilde{\delta}(\mathbf{x}) &= \nabla H(\phi(\mathbf{x})) \cdot \hat{\mathbf{n}} \\ &= H'(\phi(\mathbf{x})) \nabla \phi(\mathbf{x}) \cdot \frac{\nabla \phi(\mathbf{x})}{\|\nabla \phi(\mathbf{x})\|} \\ &= H'(\phi(\mathbf{x})) \frac{\|\nabla \phi(\mathbf{x})\|^2}{\|\nabla \phi(\mathbf{x})\|} = H'(\phi(\mathbf{x})) \|\nabla \phi(\mathbf{x})\|. \end{aligned}$$

Substituting Definition (4.17) into the last line gives

$$\tilde{\delta}(\mathbf{x}) = \delta(\phi(\mathbf{x})) \|\nabla \phi(\mathbf{x})\|. \quad (4.21)$$

By substituting Equation (4.21) into the surface integral, Definition (4.20), we get

$$\int_{\Gamma} f(\mathbf{x}) \, d\Gamma = \int_{\Omega} f(\mathbf{x}) \delta(\phi(\mathbf{x})) \|\nabla \phi(\mathbf{x})\| \, d\Omega. \quad (4.22)$$

The reason we rather use Equations (4.18) and (4.22), is to avoid identifying the interior, exterior and boundary regions of D for the calculation of the volume and boundary integrals. Instead, both integrals are taken over the entire reference domain Ω .

4.5 Implementing the level-set method

Finally, we have the knowledge to implement the level-set method into the minimum compliance problem, Problem (4.13). From the definitions of the volume integral, Definition (4.18), and surface integral, Definition (4.22), we know how to implement the level-function into the integrals of the problem.

4.5.1 Level-set embedded minimum compliance problem

Combining all this together results in the level-set embedded minimum compliance problem

$$\left\{ \begin{array}{l} \min_{\phi} \quad \tilde{a}(\mathbf{u}, \mathbf{u}, \phi) \\ \text{s.t.} \quad \tilde{a}(\mathbf{u}, \mathbf{v}, \phi) = \tilde{l}(\mathbf{v}, \phi) \quad \forall \mathbf{v} \in U_0, \\ \quad \mathbf{u}|_{\Gamma_D} = \mathbf{u}_0, \\ \quad \phi|_A = \phi_0, \\ \quad \tilde{V}(\phi) \leq V_{\max}, \end{array} \right. \quad (4.23)$$

where

$$\tilde{a}(\mathbf{u}, \mathbf{v}, \phi) := \int_{\Omega} E_{ijkl} \varepsilon_{kl}(\mathbf{u}) \varepsilon_{ij}(\mathbf{v}) (1 - H(\phi)) \, d\Omega, \quad (4.24)$$

$$\tilde{l}(\mathbf{u}, \phi) := \int_{\Omega} (\mathbf{f} \cdot \mathbf{u}) (1 - H(\phi)) \, d\Omega + \int_{\Omega} (\mathbf{t} \cdot \mathbf{u}) \delta(\phi) \|\nabla \phi\| \, d\Omega, \quad (4.25)$$

$$\tilde{V}(\phi) := \frac{\int_{\Omega} (1 - H(\phi)) \, d\Omega}{\int_{\Omega} d\Omega}. \quad (4.26)$$

Note that we no longer minimise over the design domain, but over the level-set function. That is, because the level-set function describes the design domain. By the same token, there also is a Dirichlet ‘boundary’ condition on the level-set function on the domain A .

The next step is choosing methods to solve Problem (4.23).

CHAPTER 5

SOLVING THE MINIMUM COMPLIANCE PROBLEM

The level-set based topology optimisation method described in this chapter is based on the 2015 paper of Otomori et al. [25]. They use a reaction-diffusion equation to update the level-set function. First, we must decide upon the method to solve the minimum compliance problem.

5.1 KKT conditions

We have to deal with a constrained optimisation problem, Problem (4.23). A widely used and very effective strategy for finding a local extremum subject to an equality constraint is the method of Lagrange multipliers (named after Joseph-Louis Lagrange). The Lagrangian for Problem (4.23) is given by

$$\tilde{F}[\phi, \gamma, \mathbf{v}] = \tilde{l}(\mathbf{u}, \phi) + \tilde{a}(\mathbf{u}, \mathbf{v}, \phi) - \tilde{l}(\mathbf{v}, \phi) + \gamma \left(\tilde{V}(\phi) - V_{\max} \right), \quad (5.1)$$

where γ and \mathbf{v} are the Lagrange multipliers and the displacement \mathbf{u} depends on the material distribution determined by ϕ . The vector \mathbf{v} is considered the Lagrangian parameter of the equation of motion. The Lagrangian consists of the objective functional (first term), the equation of motion in its weak form (second and third term) and the volume constraint (fourth term). Unfortunately, the inequality constraint is not suited for the method of Lagrange multipliers. Therefore, we take a look at the KKT optimality conditions (named after William Karush, Harold Kuhn and Albert Tucker), which allow inequality constraints. These KKT conditions apply to the Lagrangian

and for Problem (4.23) are as follows:

$$\begin{aligned}
 \frac{\partial \tilde{F}}{\partial \phi}[\phi, \gamma, \mathbf{v}] &= 0, \\
 \tilde{a}(\mathbf{u}, \mathbf{v}, \phi) - \tilde{l}(\mathbf{v}, \phi) &= 0, \\
 \gamma \left(\tilde{V}(\phi) - V_{\max} \right) &= 0, \\
 \gamma &\geq 0, \\
 \tilde{V}(\phi) - V_{\max} &\leq 0.
 \end{aligned} \tag{5.2}$$

In contrast to the method of Lagrange multipliers, which takes the gradient with respect to all optimisation variables and Lagrange multipliers, the first KKT condition only takes the gradient of the Lagrangian with respect to the optimisation variables. In our case, we only have one optimisation variable, ϕ , so we only have one partial derivative.

Level-set functions that satisfy these KKT conditions (5.2) are candidate solutions for the optimal level-set function that represents the optimal design. Yet, finding such level-set function solutions directly is practically impossible, aside from a few unique cases for which a closed-form solution could be derived analytically according to Boyd and Vandenberghe [10]. Therefore, we have to decide how to update the level-set function such that the KKT conditions are met.

5.2 Update procedure

The review article of Van Dijk et al. [42] mentions four update procedures: the Hamilton-Jacobi (HJ) equation, mathematical programming, the optimality criteria method and global search and gradient-free methods. These procedures determine how the level-set function is driven to the optimal solution for the optimisation problem at hand. The latter of the procedures has shown to be computationally expensive, but the others are well suited [42].

Traditionally, the level-set function is updated with a so-called Hamilton-Jacobi equation, as is done by Allaire and Jouve [3] and De Gormay [11], for example.

We introduce a generalised HJ equation, which is the standard HJ equation with a reaction and diffusion term added to it.

$$\frac{\partial \phi}{\partial \tau} - v_n \|\nabla \phi\| - \mathcal{D}(\phi) - \mathcal{R}(\phi) = 0, \tag{5.3}$$

where v_n denotes the normal velocity field and \mathcal{D} and \mathcal{R} the diffusive and reaction terms, respectively. The diffusive term gives multiple benefits. According to Van Dijk et al. [42] it “eases the numerical treatment of the HJ equation, smooths the level-set function and reduces the dependency of the optimisation results on the discretisation of the level-set function.” These are all assets we prefer our update procedure to bear. The reaction term serves as source and sink term within the material domain. This allows for the nucleation of holes.

We follow the update procedure of Otomori et al. [25] who use a generalised HJ equation without the convective term, $v_n \|\nabla \phi\|$. This makes it more a reaction-diffusion

equation than a HJ equation. As can be seen in Equation (5.3), a fictitious time τ is introduced and the optimisation problem is replaced with a time evolution equation. Thus, we consider the level-set function to be place and pseudo-time-dependent, i.e., $\phi = \phi(\mathbf{x}, \tau)$. The idea is that we iterate the level-set function, and as a result the material domain, until it convergences to the optimal design. That is, we have reached the KKT conditions.

5.2.1 Reaction-diffusion equation

Like Otomori et al. [25] we use the following reaction-diffusion equation:

$$\frac{\partial \phi}{\partial \tau} = -K \left(\frac{\partial \tilde{F}}{\partial \phi} - \alpha \Delta \phi \right) \quad \text{in } \Omega, \quad (5.4)$$

where $K > 0$ is a proportionality coefficient. Equation (5.4) is a reaction-diffusion equation, cf. Equation (5.3). The parameter α dictates the effect of the diffusivity on the evolution of the level-set function.

Adding the regularisation term makes it difficult to guarantee that the objective functional monotonically decreases. This is yet an open problem according to Otomori et al. [25].

We set appropriate boundary conditions for ϕ . This results in a boundary value problem:

$$\begin{cases} \frac{\partial \phi}{\partial \tau} = -K \left(\frac{\partial \tilde{F}}{\partial \phi} - \alpha \Delta \phi \right), & \text{in } \Omega, \\ \phi = -1 & \text{in } A, \\ \phi = -1, & \text{on } \partial\Omega_D, \\ \frac{\partial \phi}{\partial \mathbf{n}} = 0, & \text{on } \partial\Omega_N, \\ \phi(\mathbf{x}, 0) = -1, & \text{in } \Omega, \end{cases} \quad (5.5)$$

where $\partial\Omega_D := A \cap \partial\Omega$. This results in a Dirichlet boundary condition on the level-set function. On the remaining part of the boundary of the reference frame the level-set function has a homogeneous Neumann condition. So, $\partial\Omega_N := \partial\Omega \setminus \partial\Omega_D$ is considered a free boundary. Different nonhomogeneous Dirichlet boundary conditions result in different optimal designs. It is important to point out that we choose the initial value of the level-set function to be equivalent to material everywhere in the reference domain. The idea is that during the update procedure material is removed.

The next step is choosing the information we use to update the reaction-diffusion equation, Equation (5.4). There are five types of update information: variational and parameter shape sensitivities, material parameter sensitivities, topological derivatives and non-sensitivity information. The former is the most common, but uses a velocity field, which must be extended. The only type of velocity extension that supports hole nucleation is the natural extension as mentioned by Van Dijk et al. [42] in their review paper. These nucleations, however, are incidental. Since we want consistent hole-nucleation, topological derivatives are the only sufficient update information as

also pointed out by Van Dijk et al. in [42]. Therefore, a short introduction of the topological derivative is in order.

5.2.2 Topological derivative

As reported by Van Dijk et al. [42] the topological derivative of a shape functional W in a bounded domain Q is defined as:

$$d_\tau W(Q) := \lim_{r \downarrow 0} \frac{W(Q \setminus B(r)) - W(Q)}{|B(r)|}, \quad (5.6)$$

where $|\cdot|$ is a measure of the volume, and B a hole. The topological derivative is the change of a shape functional due to the introduction of an empty sphere B (or circle for $d = 2$) in the domain Q . To put it plainly, the topological derivative measures the change of the functional with respect to a change in the domain. This process is depicted in Figure 5.1. A good read on topological derivatives is the book of Novotny and Sokolowski [22].

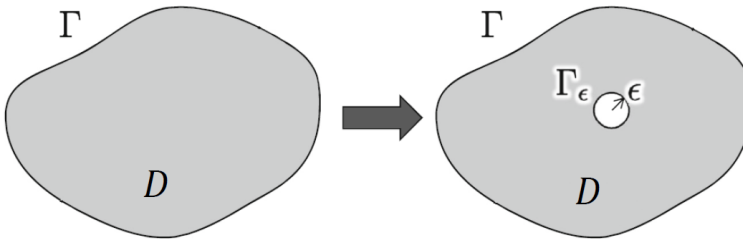


Figure 5.1: *Graphical concept of the topological derivative. Adopted by Otomori et al. [25].*

As we want to use the topological derivative to update the level-set function, we note that the partial derivative of the Lagrangian in Problem (5.5) is related to the topological derivative. Due to the material domain being defined by the level-set function, there is an equivalence between the derivative of the Lagrangian with respect to ϕ and the topological derivative of the Lagrangian. So, it is justified to replace the partial derivative of the Lagrangian with its topological derivative.

The topological derivative is problem-dependent and we use the derivation of Otomori et al. [25] for the topological derivative for the minimum compliance problem, Problem (4.23).

$$d_\tau \tilde{F}[\phi] := u_{i,j}^0 A_{ijkl} u_{k,l}^0 - \gamma. \quad (5.7)$$

Here the superscript 0 indicates the value of the displacement of the material domain without the newly created hole. The topological depends on the level-set function in the sense that the displacement is derived from the material distribution. Furthermore, the tensor A_{ijkl} is defined as

$$A_{ijkl} := \frac{3(1-\nu)}{2(1+\nu)(7-5\nu)} \left[-\frac{(1-14\nu+15\nu^2)E}{(1-2\nu)^2} \delta_{ij} \delta_{kl} + 5E(\delta_{ik} \delta_{jl} + \delta_{il} \delta_{jk}) \right]. \quad (5.8)$$

The topological derivative is calculated with the displacement of the material domain, which in turn is determined by the level-set function. The derivation of Definition (5.7) can be found in the appendix of [25].

In addition to this, we introduce a normalisation parameter C . This parameter normalises the sensitivities such that the value of α is independent of the particular problem (e.g. cantilever, MBB beam, etc.) that is being solved. The normalisation parameter is defined as

$$C := \frac{\int_{\Omega} d\Omega}{\int_{\Omega} |d_{\tau}\tilde{F}| d\Omega}. \quad (5.9)$$

In the paper of Otormori et al. [25] the parameter C has a minus sign. This is due to the fact that their material domain is represented by positive values of the level-set function. For our level-set function it is the other way around and the minus sign is left out. Moreover, Yamada et al. [46] set $K = 1$. They state that the influence of K on the dependency of the obtained optimal design is “extremely low”.

To conclude this part, we present Problem (5.5) with the topological derivative, the normalisation parameter and $K = 1$.

$$\begin{cases} \frac{\partial\phi}{\partial\tau} = -\left(Cd_{\tau}\tilde{F} - \alpha\Delta\phi\right), & \text{in } \Omega, \\ \phi = -1, & \text{in } A, \\ \phi = -1, & \text{on } \partial\Omega_{\text{D}}, \\ \frac{\partial\phi}{\partial\mathbf{n}} = 0, & \text{on } \partial\Omega_{\text{N}}, \\ \phi(\mathbf{x}, 0) = -1, & \text{in } \Omega. \end{cases} \quad (5.10)$$

The next step is discretising Problem (5.10) and solving it numerically.

5.3 Discretisation

As mentioned before, we wish to iteratively find the optimal solution for ϕ by adhering the KKT conditions. In order to achieve this, we discretise Problem (5.10) both in time and space.

5.3.1 In time

During the spatial discretisation step will we see that the diffusive term in Problem (5.10) is best treated implicitly and the topological derivative explicitly. Knowingly we chose an IMEX (implicit-explicit) finite-difference approach to update the level-set function towards the optimal solution. The level-set function at pseudo-time τ_n is denoted as $\phi(\mathbf{x}, \tau_n) = \phi^n(\mathbf{x})$, where n is the iteration step. Furthermore, $\tau^n = n\Delta\tau$, where $\Delta\tau$ is the time step for the fictitious time τ . Discretising Problem (5.10) in

time gives

$$\left\{ \begin{array}{ll} \frac{\phi^{n+1}(\mathbf{x})}{\Delta\tau} - \alpha\Delta\phi^{n+1}(\mathbf{x}) = \frac{\phi^n(\mathbf{x})}{\Delta\tau} - Cd_\tau\tilde{F}[\phi^n(\mathbf{x})], & \text{in } \Omega, \\ \phi^{n+1} = -1, & \text{in } A, \\ \phi^{n+1} = -1, & \text{on } \partial\Omega_D, \\ \frac{\partial\phi^{n+1}}{\partial\mathbf{n}} = 0, & \text{on } \partial\Omega_N, \\ \phi^0 = -1, & \text{in } \Omega, \\ \phi^0 = -1, & \text{on } \partial\Omega_D, \\ \frac{\partial\phi^0}{\partial\mathbf{n}} = 0, & \text{on } \partial\Omega_N. \end{array} \right. \quad (5.11)$$

This approach is known as the forward-backward Euler method (named after Leonhard Euler).

5.3.2 In space

We use the finite-element approach to express Problem (5.11) in its weak form. Therefore we introduce a linear test function $\tilde{b}(\mathbf{x})$ in functional space

$$\tilde{B} := \{\phi(\mathbf{x}) \mid \phi(\mathbf{x}) \in H^1(\Omega) \text{ with } \phi = 0 \text{ on } \partial\Omega_D\}.$$

Then, the weak form of Problem (5.11) for all $\tilde{b} \in \tilde{B}$ and all $n \in \mathbb{N}$ is

$$\left\{ \begin{array}{ll} \int_{\Omega} \frac{\phi^{n+1}(\mathbf{x})}{\Delta\tau} \tilde{b}(\mathbf{x}) \, d\Omega + \int_{\Omega} \alpha \nabla \phi^{n+1}(\mathbf{x}) \cdot \nabla \tilde{b}(\mathbf{x}) \, d\Omega \\ \qquad \qquad \qquad = \int_{\Omega} \left(\frac{\phi^n(\mathbf{x})}{\Delta\tau} - Cd_\tau\tilde{F}[\phi^n(\mathbf{x})] \right) \tilde{b}(\mathbf{x}) \, d\Omega & \text{in } \Omega, \\ \phi^{n+1} = -1, & \text{in } A, \\ \phi^{n+1} = -1, & \text{on } \partial\Omega_D, \\ \phi^0 = -1, & \text{in } \Omega, \\ \phi^0 = -1, & \text{on } \partial\Omega_D, \end{array} \right. \quad (5.12)$$

Notice that the second term on the left-hand side of the PDE in Problem (5.12) has been obtained after applying Gauß' divergence theorem (named after Carl Friedrich Gauß) and using the fact that $\tilde{b} = 0$ on $\partial\Omega_D$ and $\frac{\partial\phi^{n+1}}{\partial\mathbf{n}} = 0$ on $\partial\Omega_N$. In light of mathematical acknowledgement it is fair to point out that a special case of Gauß' divergence theorem is used which is known as Green's first identity (named after George Green).

We discretise System (5.12) in space using the finite-element method (FEM). We approximate the level-set function as a weighted sum of bilinear spatial basis functions with finite support:

$$\phi(\mathbf{x}, \tau_n) \approx \phi_h(\mathbf{x}, \tau_n) := \sum_{j=1}^N \phi_j(\tau_n) \tilde{b}_j(\mathbf{x}), \quad (5.13)$$

where ϕ_h is the numerical approximation of ϕ , N the number of nodes, $\phi_j(\tau_n)$ a nodal value and $\{\tilde{b}_j | \tilde{b}_j \in H^1(\Omega) \text{ for } i = 1, 2, \dots, N\}$ a set of independent basis functions. This form of parameterisation of the level-set function through the choice of basis function affects the optimisation process. For example, the support size of the basis functions can vary from local to global. We choose local basis functions, which are nonzero in a finite part of the material domain. More important is the type of basis function. The most common are FEM based basis functions, but radial basis functions (RBFs) and spectral parameterisation have been applied as well. The latter is not preferable for detailed descriptions of the material domain according to Van Dijk et al. [42]. We apply our bilinear spatial basis functions on quadrilateral elements. We choose $\tilde{b} = \tilde{b}_i$ for all $i \in \{1, 2, \dots, N\}$. Substituting this into (5.12) gives

$$\begin{cases} \underline{\mathbb{T}} \Phi_h^{n+1} = \mathbf{Y}, \\ \phi = 0 \text{ on } \partial\Omega_D, \end{cases} \quad (5.14)$$

where Φ_h^n is a vector that expresses the nodal values of the level-set function at time τ_n . The stiffness matrix $\underline{\mathbb{T}}$ and vector \mathbf{Y} in System (5.14) are defined

$$\underline{\mathbb{T}} := \bigcup_{e=1}^{N_e} \int_{V_e} \left(\frac{1}{\Delta\tau} \tilde{\mathbf{b}}^T \tilde{\mathbf{b}} + \alpha (\nabla \tilde{\mathbf{b}})^T \nabla \tilde{\mathbf{b}} \right) dV_e, \quad (5.15)$$

$$\mathbf{Y} := \bigcup_{e=1}^{N_e} \int_{V_e} \left(\frac{\phi_h(\mathbf{x}, \tau_n)}{\Delta\tau} - C d_\tau \tilde{F}[\phi_h(\mathbf{x}, \tau_n)] \right) \tilde{\mathbf{b}}^T dV_e, \quad (5.16)$$

where N_e is the number of elements and V_e is the volume of an element. $\bigcup_{e=1}^N$ represents the union set of the elements, where e is the element number. $\tilde{\mathbf{b}}$ is the row vector of basis functions.

Note that System (5.14) could also be seen as applying FEM and the backward Euler method which results in a fixed point problem because of the topological derivative term $d_\tau \tilde{F}[\phi^{n+1}(\mathbf{x})]$. Performing one Picard iteration (named after Émile Picard) gives System (5.14), where the initial fixed point estimate is taken as ϕ^n .

Equation of motion

In order to update the level-set function, the displacement of the material domain based on the current level-set function must be calculated. This displacement is used to calculate the topological derivative, Definition (5.7), and the compliance, which is twice the objective functional of Problem (4.23). Therefore, we have to solve the equation of motion. In Equation (4.11) the weak form of the equation of motion is given. We use the same FEM procedure as for the spatial discretisation of the reaction-diffusion equation. This means that we have the same basis functions, be it that they are d dimensional. In order to avoid singularities in the global stiffness matrix, we introduce an ersatz material for the void. This is common for level-set approaches and done in other works as well, e.g., Allaire and Jouve [3], and Gain and Paulino [14]. There are other ways to prevent the singularities, but using ersatz material is computationally easy to implement. Furthermore, it is worth noticing that all force

conditions of all three benchmark problems are uncomplicated and exist on that part of Γ which coincides with the boundary of the reference frame. So, we do not need to integrate over the entire reference frame as is done in Definition (4.25). We use Definition (4.12) and neglect body forces, i.e., $\mathbf{f} = \mathbf{0}$. Neglecting body forces is justified as their effect is insignificant on the scale on which we operate in combination with the material we use (steel). They would also complicate the equations we have to solve computationally.

Now, the weak form of the equation of motion becomes

$$\tilde{a}_{\text{ext}}(\mathbf{u}, \mathbf{v}, \phi) = l(\mathbf{v}), \quad (5.17)$$

where

$$\tilde{a}_{\text{ext}}(\mathbf{u}, \mathbf{v}, \phi) := \int_{\Omega} (E_{ijkl} \varepsilon_{kl}(\mathbf{u}) \varepsilon_{ij}(\mathbf{v}) (1 - H(\phi)) + E_{ijkl}^{\text{ersatz}} \varepsilon_{kl}(\mathbf{u}) \varepsilon_{ij}(\mathbf{v}) H(\phi)) \, d\Omega, \quad (5.18)$$

$$l(\mathbf{u}) = \int_{\partial\Omega} \mathbf{t} \cdot \mathbf{u} \, d\Gamma. \quad (5.19)$$

Here E_{ijkl}^{ersatz} is the same as E_{ijkl} (Definition (4.4)) except that it uses a very small Young's modulus, namely E_{\min} , which has the following property: $E_{\min} \ll E$.

A note on the calculations

The code that is used to obtain the results which are discussed in Section 5.4 is derived from the code that is presented in the paper of Otomori et al. [25]. In this code rounding errors are made when nodal values are converted to elemental value and vice versa. The topological derivative is calculated for each element. To calculate the nodal value of the topological derivative, the average value of the adjacent elements is used. To calculate the elemental level-set values, the average of the nodal values of an element is used. This average value determines whether the element in question consists of material or void. This results in a 0-1 element-wise reference domain, which is used to calculate the displacement in Equation (5.17). So, if an element has the value 1, only the first term of the integrand on the right-hand side of Definition (5.18) is used to calculate the displacement. If an element has the value 0, only the second term is used to calculate the displacement. These rounding errors have little influence on a fine mesh. However, the calculations would be more accurate if these averages were omitted. Attempts have been made to devise a better code, but this was not fruitful.

5.3.3 Bounded level-set function

We define a more specific level-set function.

Bounded level-set function

Instead of the usual definition of the level-set function, we utilise a level-set function with upper and lower limits for this method.

$$\begin{cases} -1 \leq \phi(\mathbf{x}) < 0 & \forall \mathbf{x} \in D \setminus \Gamma, \\ \phi(\mathbf{x}) = 0 & \forall \mathbf{x} \in \Gamma, \\ 0 < \phi(\mathbf{x}) \leq 1 & \forall \mathbf{x} \in \Omega \setminus D. \end{cases} \quad (5.20)$$

Again, the positive values represent the void domain, the negative values the material domain and the zero-contour the interface between the two. The upper and lower bounds are imposed on the level-set function to assure that the smoothing effect of the diffusive term only applies to points close to the boundary.

After updating the level-set function, the nodal values of the level-set function are replaced based on the following rule, such that the upper and lower limit constraints of the level-set function are satisfied:

$$\text{if } \|\phi_j\| > 1 \text{ then } \phi_j = \text{sign}(\phi_j) \quad \forall j \in \{1, 2, \dots, N\}. \quad (5.21)$$

This step can be seen as a reinitialisation step and avoids the level-set function from becoming too flat or steep. Either one could lead to convergence issues.

5.3.4 Volume constraint

As it is the most common inequality constraint in topology optimisation, a method on how to update the volume constraint and its Lagrange multiplier is presented.

The volume constraint is dealt with using the augmented Lagrangian method, in which the Lagrange multiplier γ is updated according to the following scheme:

$$\gamma_n = \frac{\int_{\Omega} (d_{\tau} \tilde{F}_n + \gamma_n) \, d\Omega}{\int_{\Omega} d\Omega} \exp \left[p \left(\frac{\tilde{G}_n}{V_{\max}} + d \right) \right]. \quad (5.22)$$

Here p and d are parameters that adjust the position of the curve and $d_{\tau} \tilde{F}_n = d_{\tau} \tilde{F}[\phi_h(\mathbf{x}, \tau_n)]$. The subscript n indicates the iteration step. Other methods to satisfy the volume constraint could be applied as well, but this scheme is simple.

We stabilise the convergence through

$$\tilde{G}_n = \tilde{V}(\phi_h(\mathbf{x}, \tau_n)) - V_{\max} - (V_0 - V_{\max}) \max \left\{ 0, 1 - \frac{n}{n_{\text{vol}}} \right\} \leq 0, \quad (5.23)$$

where n is the current iteration number and V_0 is the volume fraction of the initial material domain. The first term represents the volume of the configuration at the current iteration. The third term on the right-hand side is added to the primal volume constraint to relax the upper limit of the volume constraint so that the constraint is gradually tightened during n_{vol} iterations. After n_{vol} iterations, the constraint functional represents the original volume constraint.

5.3.5 Algorithm

In Algorithm 1 the minimum compliance process is described step-by-step.

Algorithm 1 Algorithm for minimum compliance

Require: set input values

Initialise LSF

for $n \leftarrow 1$ to n_{\max} **do**

Solve $\tilde{a}_{\text{ext}}(\mathbf{u}, \mathbf{v}, \phi^n) = l(\mathbf{v})$ for \mathbf{u} ▷ FEM (5.17)

Calculate $\tilde{a}(\mathbf{u}, \mathbf{u}, \phi^n)$ ▷ FEM (4.24)

Calculate $\tilde{V}(\phi^n)$ ▷ (4.18)

if Optimisation criteria reached **then** ▷ Criteria: $\tilde{a}(\mathbf{u}, \mathbf{u}, \phi^n)$ and $\tilde{V}(\phi^n)$

 END for loop

end if

Update $d_\tau \tilde{F}_n$ without γ_n ▷ FEM (5.7)

Update γ_n ▷ Augmented Lagrange Method (5.22)

Solve $\underline{\underline{\mathbf{T}}}\Phi^{n+1} = \mathbf{Y}$ for Φ^{n+1} ▷ IMEX and FEM (5.14)

Ensure $\|\phi^{n+1}\| \leq 1$ ▷ (5.21)

end for

return ϕ^n

Plot results

5.4 Numerical results

The moment is here to show and discuss the numerical results of all three benchmark problems. Most parameters presented in the code are known. Only the optimisation parameters that have been introduced in this chapter have yet to be assigned a value. We choose the same optimisation parameters as Otomori et al. [25], those are, in no particular order

$$\alpha = 2 \cdot 10^{-4}, \quad E_{\min} = 1 \cdot 10^{-4}, \quad \Delta\tau = 0.1, \quad d = -0.02, \quad p = 4, \quad n_{\text{vol}} = 100.$$

The value of α dictates the influence of the diffusive term in Equation (5.4). It should not be above 0.001, because then the structures do not converge or go to local minima. The time step size $\Delta\tau$ slightly influences the final design and should be chosen between 0.05 and 1. The value of d heavily influences the volume constraint. It should have a value close to 0. Choosing it to high results in not being able to attain equality (i.e. $\tilde{V} = V_{\max}$) and choosing it to low results in not being able to adhere the volume constraint at all. The other parameter p shows the same behaviour but for a wider range of values. Finally, the value of n_{vol} slightly influences the final design. It dictates how fast the volume constraint is fully enforced and how smoothly it is reached. It is preferable to choose this value such that $n_{\text{vol}} = \frac{1}{2}n_{\max}$. For every benchmark we start with material everywhere, i.e., $\phi = -1$, such that we can clearly see the nucleation of holes in the material domain.

As for the optimisation criteria, we have three criteria which must be met:

1. The number of iteration must have surpassed n_{vol} , that is $n > n_{\text{vol}}$.

2. The volume fraction of the material domain must be less than V_{\max} or differ by less than 0.5%. That is, $\tilde{V}(\phi^n) < 1.005V_{\max}$.
3. The compliance of each of the last five steps differs by less than 0.5% of the current compliance. That is, $\left| \frac{\tilde{a}(\phi^n, \mathbf{u}, \mathbf{u}) - \tilde{a}(\phi^{n-5}, \mathbf{u}, \mathbf{u})}{\tilde{a}(\phi^n, \mathbf{u}, \mathbf{u})} \right| < 0.005$ for $i \in \{1, 2, 3, 4, 5\}$.

5.4.1 MBB beam

We only take the right-hand side of the MBB beam into account, as mentioned in Chapter 3. As before, we look at the final results of a 24×8 (Figure 5.2a), 48×16 (Figure 5.2b) and 96×32 (Figure 5.2c) MBB beam. In Figure 5.2 we detect clear differences between the three designs. The boundary in Figure 5.2a is smooth, but wavy. Similar to the result of the comparative algorithm (see Figure 3.4), the structure stretches from the bottom right corner to the top left corner. The main difference is that the result of the level-set algorithm has a clear distinction between the material and the void. Furthermore, there is a small hunk of material at the bottom, which is not connected to the main structure. This discontinuity is not problematic, as it does not concern a non-free boundary point. It is, however, remarkable and probably caused by the presence of the ersatz material. When comparing Figure 5.2b to Figure 5.2a, we see that the boundary looks very smooth for the higher number of elements. Moreover, a new part of the construction has formed in the bottom left part of the reference domain. It is noteworthy that the 48 by 16 MBB beam with the level-set function looks a lot like the 96 by 32 MBB beam of the comparative algorithm (see Figure 3.6). Using even more elements results in the final design depicted in Figure 5.2c. This final design of the 96 by 32 MBB beam gives reason to believe that the structure is converging to an optimal design as it looks the same as the 48 by 16 MBB beam apart from an even smoother boundary. The resolution of the 48 by 16 MBB beam would be sufficient for industrial purposes.

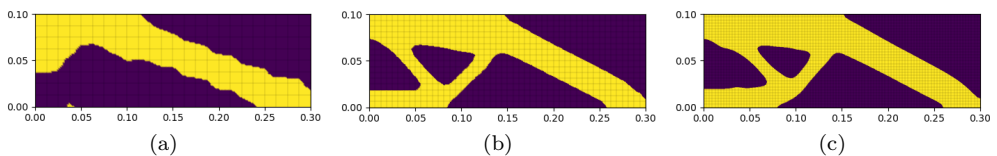


Figure 5.2: *Final designs of the MBB beam with level-set approach. (a) 24×8 ; (b) 48×16 ; (c) 96×32 . Yellow indicates material, dark blue is void.*

Figure 5.3 shows the evolution of the zero level-set curve for the different resolutions. Especially Figure 5.3c of the 96 by 32 MBB beam visualises the nucleation and merging of holes. This is an evident result of the level-set function in combination with the topological derivative.

Lastly, we look at the convergence criteria. In Figure 5.4 the compliance and volume fraction of each configuration are depicted. For every configuration the compliance mostly monotonically increases as long as the volume constraint has not been adhered. Also, the moment the volume fraction starts to decrease, the compliance shoots

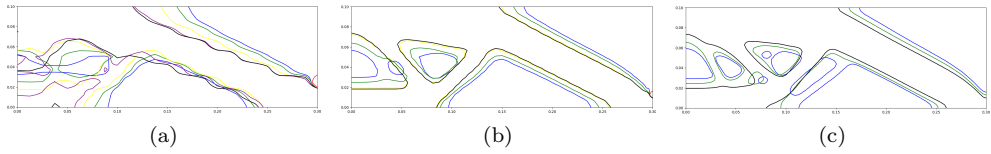


Figure 5.3: *Contour plot of the zero-level-set curve of the MBB beam. (a) 24×8 ; (b) 48×16 ; (c) 96×32 . Red: $n = 8$, blue: $n = 35$, green: $n = 70$, yellow: $n = 105$, purple: $n = 140$, brown: $n = 175$, and black is the last iteration.*

a bit up. This is a major difference in comparison to the comparative algorithm for which the objective function decreased monotonically. A reason for this can be the fact that the level-set algorithm starts with material everywhere and then material is removed. This removal of material can result in an increase of compliance, because less material has to deal with the same amount of force. Moreover, in Figure 5.4 we see that the volume constraint is satisfied for all three configurations and decreases monotonically for the two configurations with the higher number of elements. From the same figure we can also conclude that every configuration reaches the convergence criteria within 200 iterations. Figure 5.4a shows that the compliance and volume fraction converge after 155 iterations. The graph of the compliance shows huge fluctuations after 100 iterations. The 48 by 16 MBB beam adheres the convergence criteria even faster (116 iterations), which is visible in Figure 5.4b. Both graphs look smoother than the previous configuration. Figure 5.4c indicates the same behaviour for the 96 by 32 MBB beam, be it that the fluctuations are minimal. In addition to this, it converged quite fast in comparison to the other two configurations: 103 iterations.

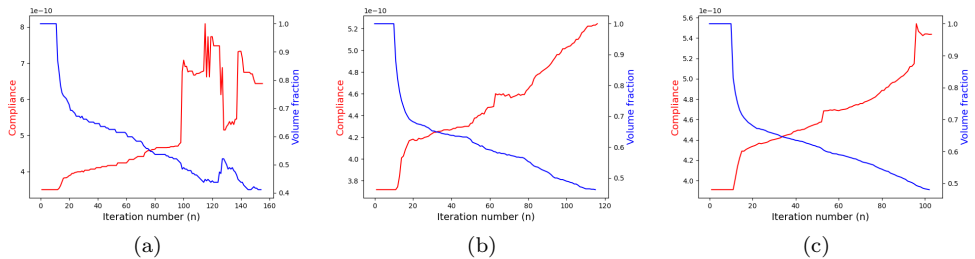


Figure 5.4: *Convergence of the compliance and volume fraction of the MBB beam with level-set approach. (a) 24×8 ; (b) 48×16 ; (c) 96×32 .*

It is also interesting to see that the final volume fraction increases as the number of elements increases too. Even so, every final volume fraction is clearly below V_{\max} .

5.4.2 Cantilever

As mentioned before, the width to height ratio of the cantilever is 2 : 1. Again we look at the results of a 16×8 (Figure 5.5a), 32×16 (Figure 5.5b) and 64×32 cantilever (5.5c). In Figure 5.5 we detect certain differences between the three designs.

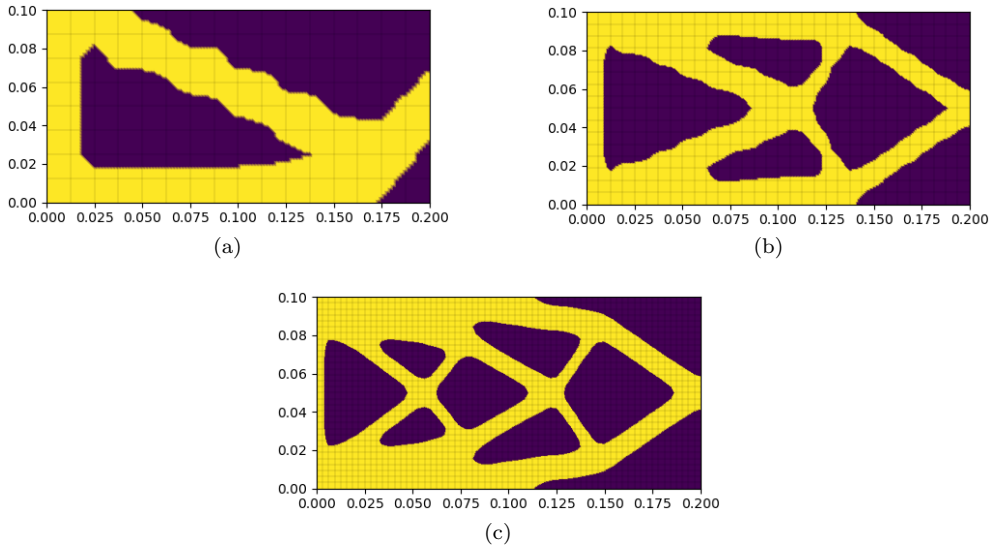


Figure 5.5: *Final designs of the cantilever with level-set approach. (a) 16×8 ; (b) 32×16 ($E_{\min} = 1$); (c) 64×32 ($E_{\min} = 1$). Yellow indicates material, dark blue is void.*

There is a curious difference between the 16 by 8 cantilever and the other two configurations. In Figure 5.5a we see that the cantilever is not symmetrical in the horizontal axis which was expected based on the results of the comparative algorithm and literature. This asymmetry can be the consequence of the very low Young's modulus of the ersatz material. If we make that Young's modulus slightly bigger ($E_{\min} = 1$), we get a symmetrical, but disconnected cantilever (see Figure 5.6a). This discontinuity is caused by the low number of elements, which is not handled well by the code. In Figure 5.6b we see the disadvantage of the 0-1 elemental domain, as mentioned in Section 5.3. For the 32 by 16 and 64 by 32 cantilevers a similar problem regarding the Young's modulus occurred. The global stiffness matrix, which is used to calculate the displacement, became singular for $E_{\min} = 1 \cdot 10^{-4}$ after a number of iterations. To this extent, we use a higher Young's modulus $E_{\min} = 1$. The 32 by 16 cantilever is similar to the cantilevers in Figure 3.10 and Figure 3.11. In Figure 5.5b we see that the boundary is more distinct although a bit wavy for some parts of the boundary. This wavy boundary disappears for a higher resolution, which can be seen in Figure 5.5c. The number of enclosed voids in the 64 by 32 cantilever is notable compared to the 32 by 16 level-set cantilever and 64 by 32 cantilever of the comparative algorithm (Figure 3.11a).

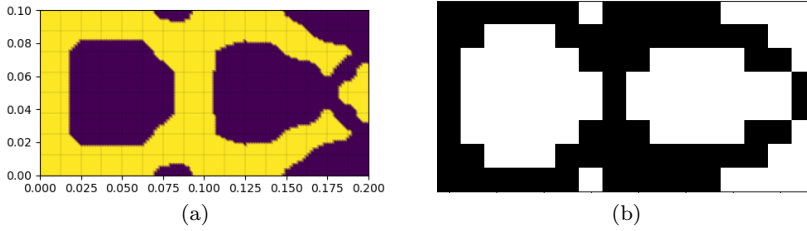


Figure 5.6: *Disconnected, symmetrical 16 by 8 cantilever with level-set approach and $E_{min} = 1$: (a) material domain (yellow indicates material, dark blue is void); (b) black (material) and white (void) plot of the 0-1 elemental domain.*

One can wonder if this number of enclosed hole rises, if the number of elements is even higher. So, we look at a 100 by 50 and a 140 by 70 cantilever. Figure 5.7 shows these final designs. Both the 100 by 50 cantilever (Figure 5.7a) and 140 by 70 cantilever (Figure 5.7b) have the same number of holes as the 64 by 32 cantilever, namely 7. This is quite remarkable, because we would expect the structure to look more like its analytic solution, which has finer features and more holes (Lewiński [18]). Although the 100 by 50 cantilever looks slightly different (smaller holes in the middle of the structure and bigger holes near the outer boundary) compared to the 64 by 32 and 140 by 70 cantilevers. The fact that the overall form and number of holes stays the same for finer meshes indicates that this level-set approach bears some kind of mesh-independency. The final designs of the MBB beam support this suspicion.

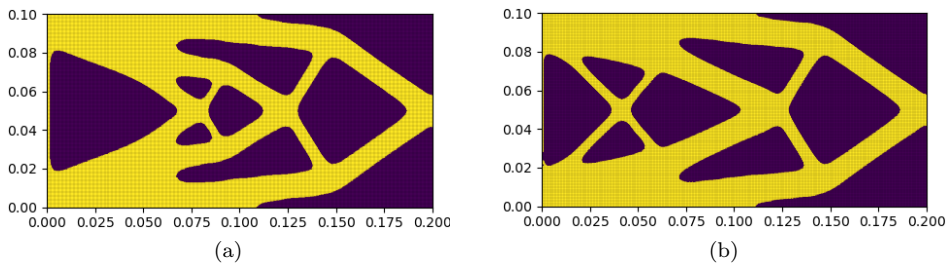


Figure 5.7: *Final design of two cantilevers on finer meshes with level-set approach and $E_{min} = 1$. Yellow indicates material, dark blue is void: (a) 100 by 50 elements; (b) 140 by 70 elements.*

In two configurations (32 by 16 and 64 by 32) in Figure 5.8 we can see the nucleation and merging of holes. The contour plots of the 16 by 8 are left out, because they are quite messy due to the asymmetry. If we look at all intermediate designs during the optimisation process of the 16 by 8 cantilever, we notice the first clear signs of asymmetry in iteration 22.

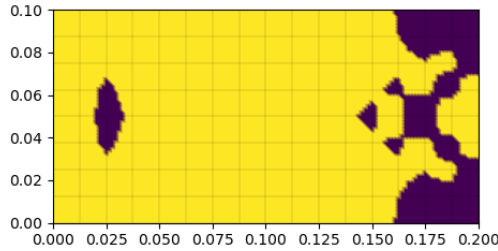


Figure 5.9: *Iteration 14 of the 16 by 8 cantilever with level-set approach. Yellow indicates material and dark blue is void.*

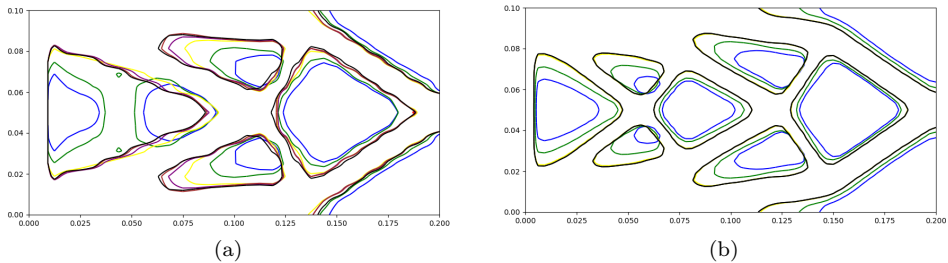


Figure 5.8: *Contour plot of the zero-level-set curve of the cantilever. (a) 16×8; (b) 32×16; (c) 64×32. Red: $n = 8$, blue: $n = 35$, green: $n = 70$, yellow: $n = 105$, purple: $n = 140$, brown: $n = 175$, and black is the last iteration.*

Lastly, we look at the convergence criteria. In Figure 5.10 the compliance and volume fraction of each configuration are depicted. The volume constraint is adhered for every configuration. What is notable is, the fact that for the 16 by 8 cantilever the compliance skyrockets when the volume fraction starts to decrease (see Figure 5.10a). After that, it falls down again. This is caused by a discontinuity in the intermediate design, as we can see in Figure 5.9

The 32 by 16 cantilever did not converge within 200 iterations, unlike the 16 by 8 cantilever, which converged after 119 iterations. Both the criterion on the volume and compliance were not met. Figure 5.10b shows that for the 32 by 16 configuration the compliance starts to fluctuate heavily after 100 iterations. The same holds for the volume fraction, but to a smaller extent. The convergence plots of the 64 by 32 cantilever, displayed in Figure 5.10c, are the smoothest in comparison to the other two configurations. Moreover, it reaches the convergence criteria the fastest: 112 iterations.

As to the final volume fractions of the MBB beam (Figure 5.4), the final volume fractions of the cantilever (Figure 5.10) are closer to V_{\max} , but also increases for a higher number of elements.

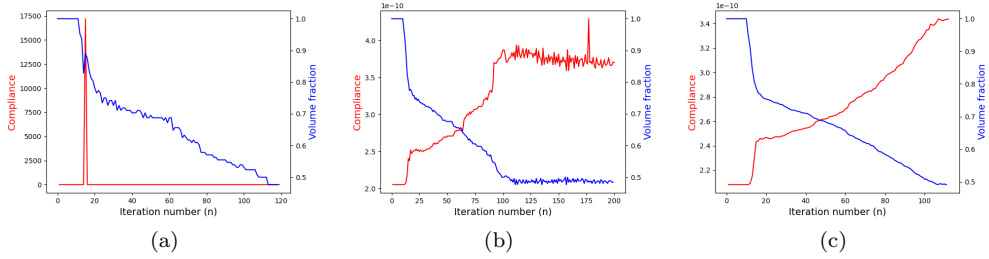


Figure 5.10: *Convergence of the compliance and volume fraction of the cantilever with level-set approach. (a) 16×8 ; (b) 32×16 ; (c) 64×32 .*

5.4.3 Inverter

As mentioned before the width to height ratio of the lower half of the inverter is $2 : 1$. We examine the results of a 16×8 (Figure 5.11a), 32×16 (Figure 5.11b) and 64×32 (Figure 5.11c) inverter. In Figure 5.11 we detect slight differences between the three designs. The boundary of the 16 by 8 inverter does not look smooth, instead it looks rugged. For the higher configurations this is not the case. Noteworthy is the size of the material on the top right corner. Every time the number of elements increases, the triangle in that corner tends to become smaller. This is a result of the smaller element size.

As we saw for the comparative algorithm, the final design is disconnected for the level-set approach as well. This gives reason to approach this problem differently.

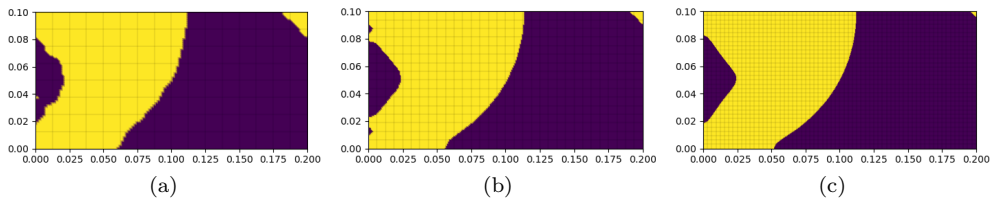


Figure 5.11: *Final designs of the inverter with level-set approach. (a) 16×8 ; (b) 32×16 ; (c) 64×32 .*

The contour plots in Figure 5.12 shows that the structure has already a huge discontinuity between the left part and right part of the structure after 8 iterations. This indicates that the structure breaks very early during the optimisation process.

Lastly, we look at the convergence criteria. In Figure 5.14 the compliance and volume fraction of each configuration are depicted. For all three configurations the volume fraction drops quite steep compared to the other two benchmark problems. At the same time the compliance makes a steep climb. This happens after 11 iterations and might be caused by a discontinuity in structure.

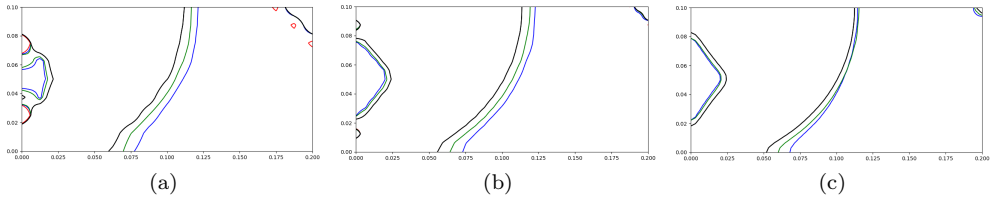


Figure 5.12: *Contour plot of the zero-level-set curve of the inverter. (a) 16×8 ; (b) 32×16 ; (c) 64×32 . Red: $n = 8$, blue: $n = 35$, green: $n = 70$, yellow: $n = 105$, purple: $n = 140$, brown: $n = 175$, and black is the last iteration.*

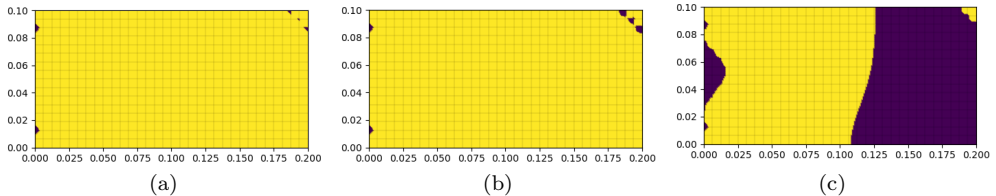


Figure 5.13: *Iterations steps of the 32 by 16 inverter. After (a) 10 iterations; (b) 11 iterations; (c) 12 iterations.*

Figure 5.13 indeed confirms that the breakup occurs after 11 iterations. In Figures 5.13a and 5.13b we see that three holes are forming in the top right corner. During the 11th (Figure 5.13c) a huge part of the material is removed. This explains the drop in the volume fraction and rise in the compliance, which we detected earlier.

Unlike the MBB beam and cantilever, the volume fraction of the inverter drops below V_{\max} to a value slightly lower than 0.4. This is very strange, because from Figure 5.14c we can deduce that the optimal design is achieved after 50 iterations. After 50 iterations the volume constraint is adhered and the compliance is in a local minimum. On another note, the staircase-like graph of the compliance in Figure 5.14a is unusual as well. Both irregularities could be caused by the Lagrangian γ .

In contrast to the final volume fractions of the MBB beam (Figure 5.4) and cantilever (Figure 5.10), the final volume fractions of the inverter decrease as the number of elements increases. This is a result of the convergence criterion on the number of iterations that should have passed, namely more than n_{vol} . Because of the breakup, the volume constraint is reached very fast and the role of n_{vol} becomes obsolete. We can consider this to be a drawback of this specific choice of convergence criterion.

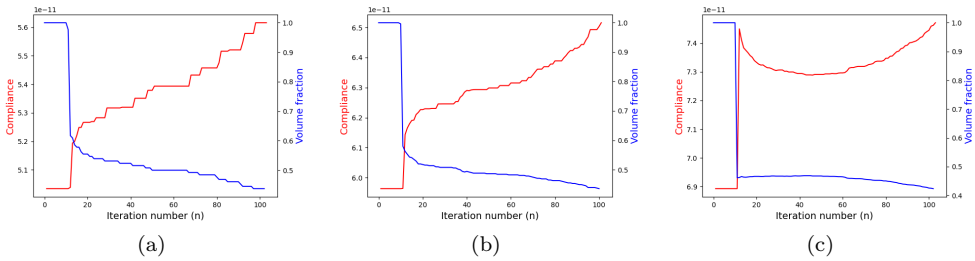


Figure 5.14: *Convergence of the compliance and volume fraction of the inverter with level-set approach. (a) 16×8 ; (b) 32×16 ; (c) 64×32 .*

Cause of the breakup

The reason the top right corner point is not connected to the main structure in the final designs of both the SIMP and level-set approach is that there is not explicit constraint on this connectivity. There is no physical reason that this top right corner point should be connected through material to the other two points of interest. This is because there is no mechanical condition on this top right corner point which would result in a boundary condition on the displacement. Moreover, because there is no mechanical condition, there is also no reason there should be material present in that particular point. Now, if we would fix this top right corner point, there is a justification for the presence of material in that point. In Figure 5.15 we see the final designs of the inverter if the point is fixed. We see that the structure is now entirely connected through material. That is because there is a physical reason to connect that point to the other two point with predefined material. The force pointed to the right is intercepted by the fixed point on the right.

So, the final designs shown in Figures 3.17, 3.18, 3.19 and 5.11 are actually the correct optimal designs for the minimum compliance problem as there is no explicit constraint on the connectivity of the structure. Using the level-set approach does not change the final design or fix this discontinuity compared to the SIMP approach. Now, we have reason to investigate the possibilities of incorporating an explicit connectivity constraint into the algorithm.

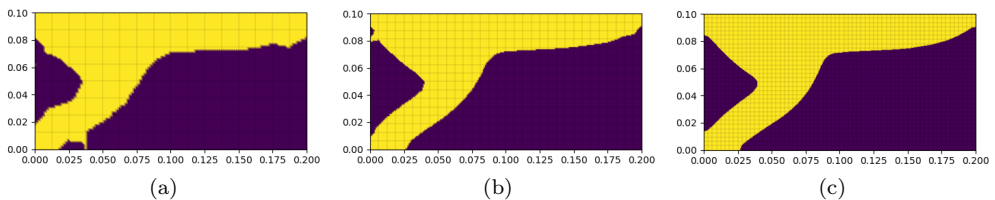


Figure 5.15: *Inverter with fixed top right corner point.*

CHAPTER 6

CONNECTIVITY

As we saw in Chapters 3 and 5, it is possible that the structure breaks and does not obtain a desired optimal design. This happened for the inverter problem with both the SIMP approach (Figure 3.20) and level-set approach (Figure 5.11). In this chapter we look at the possibilities to prevent this ‘breakdown’ from occurring during the optimisation process by explicitly defining a connectivity constraint. Only the two dimensional case is treated in this chapter.

6.1 Path connectedness

Instead of looking at the problem in terms of breaking, we look at it in terms of connectivity. We desire some sort of connectedness to be present in our optimal design. For example, a structure is called *simply-connected* if there are no enclosed voids present in the material domain. We, however, allow our design to have these enclosed voids. We even chose our update procedure such that these holes can be nucleated. The type of connectivity we are interested in is mentioned in the 2011 paper of Kasaiezadeh and Khajepour [16]. They call a structure *generally connected* “when there is at least one path to connect the location of the applied force to the geometrical boundary conditions”. The author of this thesis has altered this definition slightly and taken multiple forces into account. A structure is called *path connected* if there is a material path connecting every non-free boundary point with every other non-free boundary point. This definition does not include the non-free boundary points which have a homogeneous Dirichlet boundary condition due to a symmetry axis. So, this definition concerns all points in $\partial\Omega_N$. Using the set A would even be better, because we want all points where we have material a priori to be path connected. This includes points in the interior of A as well. Otherwise, it would be redundant to have material in those points. For our benchmarks, however, we have $\partial\Omega_N = A$.

6.2 Detection algorithm

First, we want to know how we can detect that a design is path connected. If we know that, we also know when it is no longer path connected. During every iteration of the optimisation process the path connectedness should be checked, because then we know the exact moment the structure becomes disconnected. Knowing this moment gives room for a prevention method.

Now, we must think of an algorithm that is able to systematically check the path connectedness. Because the location of each force must be connected to all Dirichlet boundary conditions, all forces are connected to each other as well. Therefore, we do not have to make a difference between a force on the boundary or a Dirichlet boundary condition. They all have to be connected. A boundary force or Dirichlet condition is either on a boundary node or an entire boundary element edge. If it is on a node, the adjacent elements are called m_b elements. If it is on an edge, the element to which this edge belongs is called an m_b element. Moreover, we know that this node or edge must consist of material.

Now, we create a number of empty lists: L_{path} , L_{check} , L_{new} and L_{con} . We put all m_b elements in L_{path} . Then we select one of these elements at random and call it m_0 . This is the element from where the path connectedness detection algorithm starts. The m_0 element is taken from L_{path} and put into L_{new} .

6.2.1 Detection loop

The detection loop starts by checking for every element in L_{new} if it is connected through material to its neighbouring elements. To make sure we do not double check any elements, we do not check elements that are in L_{check} . We look at how this check is performed for one single neighbour.

As we apply FEM to calculate the level-set function during each iteration step, we utilise the fact that we have linear basis functions on either triangular or quadrilateral elements. The shared edge of the two elements has two nodal values of the level-set function. There are three cases to distinguish:

1. Both nodal values of the level-set function are negative. This indicates that the entire edge consists of material.
2. One of the two nodal values of the level-set function is nonnegative. This indicates that the zero level-set curve goes through the edge (including the nodes). So, part of the edge consists of material.
3. Both nodal values of the level-set function are nonnegative. This indicates that no part of the boundary consists of material.

It is important to remark that these statements only hold for linear basis functions. In the first and second case we say the two elements are connected. In other words, if one of the two nodes is negative, the two elements are connected. After this check has been completed for every neighbour that is not in L_{check} , we put every newly connected neighbour element in L_{con} . Now, we move all elements from L_{new} to L_{check}

and all elements from L_{con} to L_{new} . Then, we check whether path connectedness has been achieved by looking whether all elements of L_{path} are in either L_{check} or L_{new} . If not, the detection loop is repeated until path connectedness is achieved. The detection loop also stops when no more elements are added to L_{new} . If this is the case, a breakdown has occurred and the structure is not path connected.

6.2.2 False positive

For the quadrilateral elements there is a situation in which two elements are connected through a third element with the current algorithm described above while they should not be. This can be seen as a false positive. An example of this situation is depicted in Figure 6.1. The problem is caused by ‘elm₅’ which has two negative level-set values on opposite vertices and the same for two positive level-set values. In this specific setting the algorithm would first connect ‘elm₄’ with ‘elm₅’ and in the next step connect ‘elm₅’ to ‘elm₆’. This means that ‘elm₄’ is connected with ‘elm₆’ which is not correct. This problem does not occur if triangular elements are used in the finite-element method.

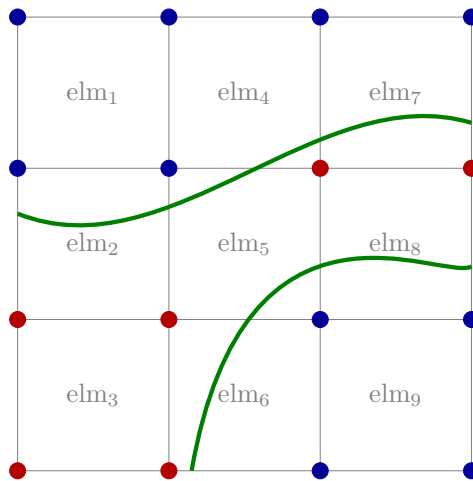


Figure 6.1: *Graphical example of a false positive. The red and blue dots indicate positive and negative level-set values, respectively. The zero level-set curve is represented by green lines.*

As the problem occurs in ‘elm₅’, we brief focus on this specific element. Henceforth, we refer to such an element as a *false positive*.

Solution

A solution to the false positive problem has been found by the author and is explained thoroughly. We consider a quadrilateral element with alternating nodal level-set values. For simplicity, we assume that the quadrilateral is the unit square. A random quadrilateral can easily be converted to a unit square (see [44]). Starting with $(0, 0)$

and going counterclockwise, the nodal level-set values of the vertices are called a_1 , a_2 , a_3 and a_4 . We do not know before hand which vertices of the unit square are negative and which are positive. We only know that the values of a_1 , a_2 , a_3 and a_4 are alternating in sign. The corresponding basis functions are

$$\begin{aligned}\tilde{b}_1(x, y) &= (1 - x)(1 - y), \\ \tilde{b}_2(x, y) &= x(1 - y), \\ \tilde{b}_3(x, y) &= xy, \\ \tilde{b}_4(x, y) &= (1 - x)y.\end{aligned}\tag{6.1}$$

From this we derive the approximate the level-set function in this single element based on Definition (5.13),

$$\phi_h(x, y) = (a_1 - a_2 + a_3 - a_4)xy + (a_2 - a_1)x + (a_4 - a_1)y + a_1.\tag{6.2}$$

As we are interested in how the zero level-set curve behaves in the unit square element, we equate Expression (6.2) to zero. This equation can be viewed as a *general quadratic equation* as described by Zwillinger in his book [47]:

$$Ax^2 + By^2 + Cxy + Dx + Ey + F = 0,\tag{6.3}$$

where

$$\begin{aligned}A &= 0, \\ B &= 0, \\ C &= a_1 - a_2 + a_3 - a_4, \\ D &= a_2 - a_1, \\ E &= a_4 - a_1, \\ F &= a_1.\end{aligned}\tag{6.4}$$

Remark that, as a result of the alternating signs of a_1 , a_2 , a_3 and a_4 , we know that C, D, E and F are never zero. Zwillinger [47] gives a table which can be used to determine the type of conic at hand. For this table he uses four quantities derived from Equation (6.3). For our level-set function in Expression (6.2) these quantities are

$$\Delta = \frac{1}{4}C(DE - CF),\tag{6.5}$$

$$J = -\frac{1}{4}C^2 < 0,\tag{6.6}$$

$$I = 0,\tag{6.7}$$

$$K = -\frac{1}{4}(D^2 + E^2) < 0.\tag{6.8}$$

Note that we used that $A = B = 0$ and that C, D, E and F are nonzero. Now, if we look at the table of the different types of conics in the book of Zwillinger [47], we see that the only possible types are a hyperbola or intersecting lines, which both require

$J < 0$. In Figures 6.2a and 6.2b two cases of the hyperbola are depicted. The first shows that the quadrilateral is connected internally and to all its neighbours. The latter shows that the material is internally disconnected. Figure 6.2c shows the intersecting lines. In this case the element is also internally disconnected, as neither the material nor the void is connected.

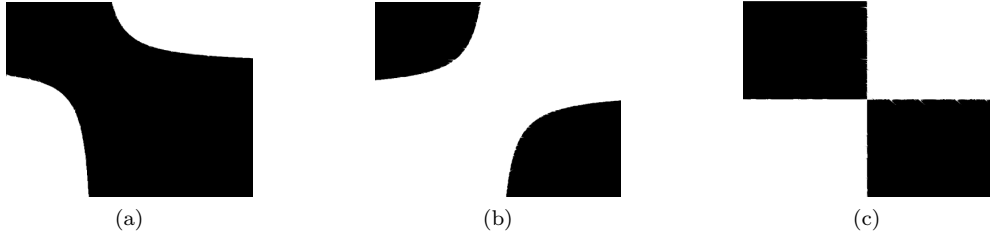


Figure 6.2: *Three situations of the material distribution in element with alternating nodal level-set values. (a) hyperbola (connected); (b) hyperbola (disconnected: false positive); (c) tipping point (disconnected: false positive).*

Intersecting lines only occur if $\Delta = 0$, which implies that $DE = CF$ (since $C \neq 0$). In terms of the nodal level-set values this comes down to

$$a_1 a_3 = a_2 a_4. \quad (6.9)$$

However, we want to know if the quadrilateral element is a false positive or not. Therefore, we look at the centre (x_0, y_0) of the hyperbola. We assume that if this centre is in the material, i.e., $\phi_h(x_0, y_0) < 0$, the quadrilateral element is internally connected. According to Zwillinger [47], the coordinates of this centre are the solution of the following system of equations:

$$\begin{cases} 2Ax + Cy + D = 0, \\ Cx + 2By + E = 0. \end{cases} \quad (6.10)$$

So, for our bilinear level-set approximation the coordinates of the centre are given by

$$x_0 = -\frac{E}{C}, \quad y_0 = -\frac{D}{C}. \quad (6.11)$$

We substitute the coordinates of Expression (6.11) into the general quadratic equation of the zero level-set curve, Equation (6.2). This results in the following expression:

$$\phi_h(x_0, y_0) = F - \frac{DE}{C}. \quad (6.12)$$

Finally, an element with alternating nodal level-set values is called *internally connected* if and only if

$$\frac{a_1 a_3 - a_2 a_4}{a_1 - a_2 + a_3 - a_4} < 0. \quad (6.13)$$

Notice that if an element is internally connected, the possibility of intersecting lines (see Equation (6.9)) is automatically ruled out, because the numerator of Inequality (6.13) is nonzero. An element that has alternating nodal level-set values but does not adhere Inequality (6.13) is called *internally disconnected*.

The next step is implementing this knowledge into the algorithm. The most simple way is by selecting all elements with alternating nodal level-set values and check if they adhere Inequality (6.13). If not, they are placed in L_{check} . This prevents them from being checked as potential connected neighbours, because elements in L_{check} are considered checked and are not checked again during the main algorithm. However, if the element in question is an m_b element, placing it in L_{check} would cause problems, if it is also in L_{path} . Simply transferring them from L_{path} to L_{check} solves the problem. However, we can make the detection algorithm substantially faster if we perform a special check on the m_b elements before we possibly transfer them. First, we take a look at the problems that might occur if we do not place m_b element in L_{check} .

6.2.3 Problems with m_b elements

Boundary elements which have a node on which a Dirichlet or force boundary condition is defined are treated differently. They are called m_b elements and are placed in L_{path} , before detection loop starts. One of these m_b elements is chosen as the starting point (placed in L_{new}) of this loop which can cause problems if this element is internally disconnected. Note that these problems only occur for nodal boundary conditions. We take a look at these problematic cases.

We start by looking at a Dirichlet or force boundary condition on a node on a corner of the reference frame. If this element is internally disconnected (Figure 6.3) or has three positive nodal level-set values (Figure 6.4) than we know beforehand that the structure is not path connected. The corner point is automatically isolated from the rest of the structure. In the case of internally disconnectedness, the detection loop would start without any problems because the corner element is in L_{new} and not in L_{check} . This is problematic, because the algorithm does not detect that the structure is not path connected.

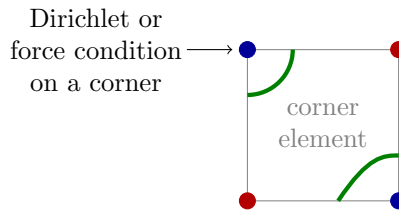


Figure 6.3: *Graphical example of a corner node with a Dirichlet or force boundary condition on an internally disconnected element. The red and blue dots indicate positive and negative level-set values, respectively. The zero level-set curve is represented by green lines.*

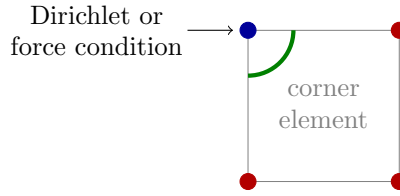


Figure 6.4: *Graphical example of a corner node with a Dirichlet or force boundary condition on an element with three positive nodal level-set values. The red and blue dots indicate positive and negative level-set values, respectively. The zero level-set curve is represented by green lines.*

Now, we look at a boundary node that is not on a corner of the reference domain. In this case there are two adjacent elements which are placed in L_{path} . If one of the two elements is internally disconnected as depicted in Figure 6.5, then this element can wrongly be chosen as the starting point. Then, the same problem as for the internally disconnected corner element occurs.

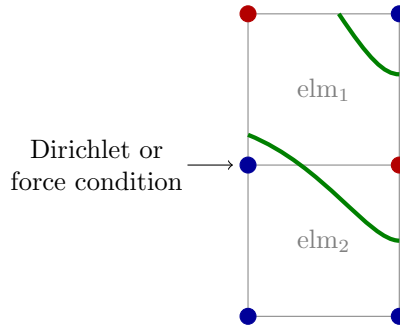


Figure 6.5: *Graphical example of boundary node with a Dirichlet or force condition with one internally connected and one disconnected adjacent element. The red and blue dots indicate positive and negative level-set values, respectively. The zero level-set curve is represented by green lines.*

In the case that both adjacent elements are internally disconnected, the node with a Dirichlet or force condition becomes isolated, as we can see in Figure 6.6. So, there is no reason to start the detection loop as the structure is already not path connected at this nodal point.

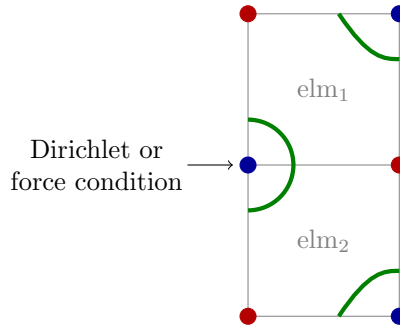


Figure 6.6: *Graphical example of a boundary node with two internally disconnected adjacent elements. The red and blue dots indicate positive and negative level-set values, respectively. The zero level-set curve is represented by green lines.*

In order to keep the detection algorithm neat, we have to change the definition of the m_b elements. A special check has to take place before an element can be defined as m_b element. Problems could only occur for Dirichlet boundary or force conditions on nodes, so all elements which have an edge with a Dirichlet boundary or force condition on it are defined to be m_b elements.

If we encounter a nodal boundary or force condition on a corner of the reference frame, we look at the corresponding corner element. If it has three positive level-set values, a breakdown has occurred and no path connectedness can be detected. If it has alternating nodal level-set values, we check if Inequality (6.13) is adhered. If this is not the case, a breakdown has occurred and no path connectedness can be detected. If the inequality is adhered, the corner element is defined as m_b element. In any other case the corner element is also defined as m_b element.

If we encounter a nodal boundary or force condition that is not on a corner of the reference frame, this means that there are two adjacent elements. If one of the two elements has alternating nodal level-set values and does not adhere Inequality (6.13), this element is placed in L_{check} and the other defined as m_b element. If both elements have alternating nodal level-set values, there are three possibilities:

1. Both elements do not adhere Inequality (6.13) and a breakdown has occurred which implies that no path connectedness can be detected.
2. One of the two elements does not adhere Inequality (6.13). This element is placed in L_{check} and the element that does adhere the inequality is defined as m_b element.
3. Both elements adhere Inequality (6.13), they are both defined as m_b elements.

In any other case the the adjacent elements are also defined as m_b elements.

6.2.4 Two diagonal internally connected elements

Two elements, which have alternating nodal level-set values and are internally connected, can be diagonally connected with each other, if the other two adjacent neigh-

bour elements also have alternating nodal level-set values but are internally disconnected. This diagonal connection, however, will not be detected by the current algorithm because the internally disconnected neighbour elements are excluded from the path. An example of this type of problem is illustrated in Figure 6.7. In this case the problem occurs between the two internally connected elements ‘elm₅’ and ‘elm₉’. They do not connect because the two adjacent internally disconnected elements ‘elm₆’ and ‘elm₈’ are excluded from checking as they have already been placed in L_{check} before the detection loop has commenced.

Fortunately this problem is easily solved. For each element, which has alternating nodal level-set values and is internally connected, we check if its diagonal neighbours are internally connected as well. If this is indeed the case the diagonal neighbour is added to L_{con} .

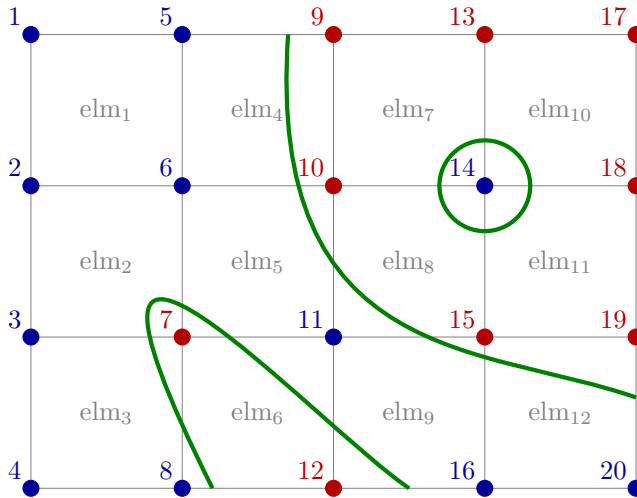


Figure 6.7: Graphical example of two diagonally connected elements. The red and blue dots indicate positive and negative level-set values, respectively. The zero level-set curve is represented by green lines.

6.2.5 Final detection algorithm

Now, taking everything into account regarding internally connected and disconnected elements, and the definition of m_b elements, the final algorithm to detection path connectedness is presented in pseudo-code in Algorithm 2.

Algorithm 2 Final algorithm for path connectedness

Require: B.C., forces, topology, nodal level-set values

Create empty lists: L_{path} , L_{check} , L_{new} and L_{con}

Put all m_b force and boundary elements in L_{path}

False positive elements not in L_{path} are placed in L_{check}

Select one element from L_{path} at random and call it m_0

Place m_0 in L_{new}

while L_{new} is nonempty **do**

for each element m_0 in L_{new} **do**

for each neighbour m_1 that is not in L_{check} **do**

if at least one of the two corresponding nodes is negative **then**

 Add m_1 to L_{con}

end if

end for

if m_0 is internally connected **then**

for each diagonal neighbour m_1 with a corresponding negative node **do**

if m_1 is internally connected **then**

 Add m_1 to L_{con}

end if

end for

end if

end for

Move all elements from L_{new} to L_{check}

Move all elements from L_{con} to L_{new}

if all elements of L_{path} are in the union of L_{check} and L_{new} **then**

 Path connectedness detected

end if

end while

No path connectedness detected

6.3 Prevention

We could also try to prevent the structure from ever losing its path connectedness or enable the algorithm to regain it. Kasaiezadeh and Khajepour [16] imposed an extra inequality constraint which secured path connectedness. They looked at what would physically happen if the structure would lose its path connectedness and concluded that the strain energy increases significantly in the void (which consists of ersatz material). Indeed, in Figure 6.8 we see that the strain energy density increases extremely for the 32 by 16 inverter during the twelfth iteration, the moment the intermediate design breaks.

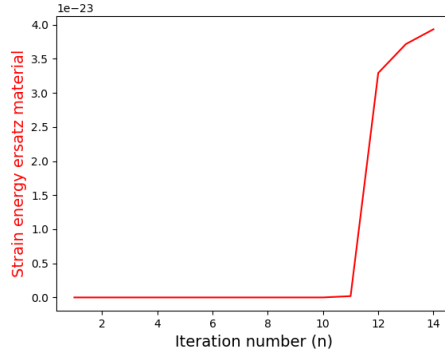


Figure 6.8: *Plot of the strain energy ersatz material of the 32 by 16 inverter with the level-set approach.*

Despite the volume fraction of the void increasing, the strain energy in the ersatz material increases absurdly after the breakup. The strain energy goes from $1.95 \cdot 10^{-25}$ to $3.29 \cdot 10^{-23}$, which is almost a factor 169 bigger. It is worth mentioning that the strain energy in the ersatz material also increase when a hole is formed, but not as sharply as in the case of a breakup. So, by imposing a limit on the total strain energy in the void of the structure, Kasaiezadeh and Khajepour [16] retained generally connectedness.

The inequality constraint on the strain energy in the ersatz material is defined as

$$\tilde{S}(\mathbf{u}, \mathbf{v}, \phi) := \int_{\Omega} E_{ijkl}^{\text{ersatz}} \varepsilon_{kl}(\mathbf{u}) \varepsilon_{ij}(\mathbf{v}) H(\phi) \, d\Omega \leq S_{\max}, \quad (6.14)$$

where S_{\max} denotes the upper bound for the strain energy. Note the similarities with the energy bilinear term (cf. (4.24)). There are, however, two important differences. First, the integral is zero over the material domain due to the use of $H(\phi)$ instead of $(1 - H(\phi))$. Second, the elasticity tensor corresponds with the ersatz material, i.e. the Young's modulus is very small. Notice that we can express Definition (5.18) as

$$\tilde{a}_{\text{ext}}(\mathbf{u}, \mathbf{v}, \phi) = \tilde{a}(\mathbf{u}, \mathbf{v}, \phi) + \tilde{S}(\mathbf{u}, \mathbf{v}, \phi).$$

A serious drawback of this inequality constraint is that one has to determine the value of this upper bound S_{\max} . This value differs for every problem and material. Moreover, if a structure would obtain its optimal, path connected design without using this constraint, then using it during the entire optimisation process could effect the final design. In other words, this inequality constraint could make the structure converge locally instead of globally. That is why Kasaiezadeh and Khajepour choose to use the functional \tilde{S} in their Lagrangian only if the upper bound is exceeded.

6.4 Combining detection and prevention

Now the following idea has occurred to the author. We use the detection algorithm parallel to the optimisation process. During each iteration the path connectedness is

checked. If the algorithm detects that there is no longer path connectedness, we go back one iteration and impose the strain energy inequality, Inequality (6.14), on the minimum compliance problem, Problem (4.23). This should secure the path connectedness for that step. To determine the value of S_{\max} we use the known strain energy in the ersatz material, $\tilde{S}(\phi)$, before and after the occurrence of the discontinuity in the following way:

$$S_{\max} := \frac{\tilde{S}(\phi^{n+1}) + \tilde{S}(\phi^n)}{2}. \quad (6.15)$$

Here ϕ^n denotes the level-set function before the breakup and ϕ^{n+1} after. An observant reader recognises the arithmetic mean in this definition. As there is no accurate way to predict S_{\max} a priori, we have to estimate it during the iteration process. Because we have the value of $\tilde{S}(\phi)$ before and after the structure disconnects, we know that S_{\max} should be between those two values. The arithmetic mean is an acceptable estimator in this case, as we do not want to spend too much time on finding the exact value. A disadvantage of simply using $\tilde{S}(\phi^n)$ as S_{\max} is that the value might be too far of the actual S_{\max} and this could result in a suboptimal final design. If the estimation of S_{\max} is too high, the structure will break again and we can find a lower value with Definition (6.15) again based on the new broken structure. The new value of S_{\max} could be higher than its previous value. This is not something we want and therefore we redefine S_{\max} slightly,

$$S_{\max} = \min \left\{ \frac{\tilde{S}(\phi^{n+1}) + \tilde{S}(\phi^n)}{2}, S_{\max} \right\}. \quad (6.16)$$

Before the optimisation loop we set $S_{\max} = \infty$. If the value of S_{\max} is low enough, the structure will not break and we can continue the iteration process.

Imposing this constraint will alter the Lagrangian and therefore the topological derivative. The Lagrangian becomes

$$\tilde{P}[\mathbf{u}, \mathbf{v}, \phi, \gamma, \beta] := \tilde{l}(\mathbf{u}, \phi) + \tilde{a}(\mathbf{u}, \mathbf{v}, \phi) - \tilde{l}(\mathbf{v}, \phi) + \gamma \left(\tilde{V}(\phi) - V_{\max} \right) + \beta \left(\tilde{S}(\mathbf{u}, \mathbf{v}, \phi) - S_{\max} \right), \quad (6.17)$$

where β is an extra Lagrange multiplier for the inequality constraint on the strain energy in the ersatz material. The topological derivative becomes

$$d_{\tau} \tilde{P} := u_{i,j}^0 A_{ijkl} u_{k,l}^0 - \beta u_{i,j}^0 A_{ijkl}^{\text{ersatz}} u_{k,l}^0 - \gamma. \quad (6.18)$$

Here A_{ijkl}^{ersatz} is the same tensor as A_{ijkl} , but it has a different Young's modulus and is nonzero in the void. Note that the calculation of this alternative topological derivative does not result in any extra computational effort as we already have calculated the displacement in the material and ersatz material (see Equation (5.17)). Similar to γ_n the new Lagrangian multiplier for the strain energy constraint should be updated as well. The Lagrangian β_n is updated according to the following scheme:

$$\beta_n = \max \left\{ \frac{\tilde{S}(\phi^{n+1}) - S_{\max}}{S_{\max}}, 0 \right\}. \quad (6.19)$$

The reason we choose for this scheme is that it becomes zero when $\tilde{S}(\phi^{n+1})$ is smaller than S_{\max} . This could happen when the value of S_{\max} is too high. In addition to

this, we want β to depend on S_{\max} and the strain energy in the ersatz material of the broken structure. So, we chose the relative difference between the two, because it takes the ‘size’ of the quantities into account. Now that the topological derivative is different than before, we have to update the Lagrangian for the volume constrain, γ , as well. The Lagrangian γ_n is updated according to the following scheme:

$$\gamma_n = \frac{\int_{\Omega} (d_{\tau} \tilde{P}_n + \gamma_n) \, d\Omega}{\int_{\Omega} d\Omega} \exp \left[p \left(\frac{\tilde{G}_n}{V_{\max}} + d \right) \right], \quad (6.20)$$

where \tilde{G}_n is the same as in Definition (5.23). Note that only the topological derivative is different.

After the Lagrangian of Definition (6.17) and the topological derivative of Definition (6.18) have been used for one iteration and secured path connectedness, the following iteration step uses the original Lagrangian of Definition (5.1) and topological derivative of Definition (5.7) again. The detection algorithm is active during every iteration step.

At last, we have derived a new algorithm to solve the level-set embedded minimum compliance problem, Problem (4.23). Compared to the previous algorithm, Algorithm 1, this new algorithm, Algorithm 3 detects if there is no path connectedness and in that case can prevent it.

6.5 Results of the new algorithm

The results, which were provided by Algorithm 3, were unsatisfactory and quite strange. The algorithm behaves unpredictable. It first removes material, then adds material, for one iteration it regains path connectedness and eventually removes all material, except for the points in A . This can be seen in Figure 6.9. Moreover, the value of S_{\max} becomes extreme: zero. This causes β to become infinity. This suggests that the Algorithm 3 does not work as intended. The problem probably lies in the fact that this algorithm wants to achieve path connectedness in one iteration step. This is in contrast with the manner in which the volume constraint is achieved. To adhere the KKT condition for the volume constraint, Algorithm 1 takes a huge amount of iterations to reach it. It is very plausible that path connectedness should be regained in the same manner.

6.5.1 Alternative prevention algorithm

Although there is no time left to test, the author would like to suggest a restoration algorithm that might work. Instead of trying to secure path connectedness in one iteration step, we give the algorithm ‘time’ to restore path connectedness similar to how the volume constraint is reached. So, if the path connectedness is lost, the algorithm calculates β and includes the strain energy constraint in the Lagrangian. Different from Algorithm 3, this new algorithm only uses the level-set function from before the breakup to calculate S_{\max} . Instead of calculating β_n , the displacement and $d_{\tau} \tilde{P}_n$ based on the last unbroken ϕ , we use the updated level-set function even though it has no path connectedness. This means that the definition of the upper bound for the

Algorithm 3 Algorithm for minimum compliance with detection and prevention

Require: set input values

Initialise LSF

$S_{\max} = \infty$

for $n \leftarrow 1$ to n_{\max} **do**

Solve $\tilde{a}_{\text{ext}}(\mathbf{u}, \mathbf{v}, \phi^n) = l(\mathbf{v})$ for \mathbf{u} ▷ FEM (5.17)

Calculate $\tilde{a}(\mathbf{u}, \mathbf{u}, \phi^n)$ ▷ FEM (4.24)

Calculate $\tilde{V}(\phi^n)$ ▷ (4.18)

if Optimisation criteria reached **then** ▷ Criteria: $\tilde{a}(\mathbf{u}, \mathbf{u}, \phi^n)$ and $\tilde{V}(\phi^n)$

 END loop

end if

Update $d_\tau \tilde{F}_n$ without γ_n ▷ FEM (5.7)

Update γ_n ▷ Augmented Lagrange Method (5.22)

Solve $\underline{\underline{\mathbf{T}}}\Phi^{n+1} = \mathbf{Y}$ for Φ^{n+1} ▷ IMEX and FEM (5.14)

Ensure $\|\phi^{n+1}\| \leq 1$ ▷ (5.21)

Check path connectedness ▷ Algorithm 2

while Path connectedness is false **do**

 Solve $\tilde{a}_{\text{ext}}(\mathbf{u}, \mathbf{v}, \phi^{n+1}) = l(\mathbf{v})$ for \mathbf{u} ▷ FEM (5.17)

 Calculate $\tilde{S}(\phi^n)$ and $\tilde{S}(\phi^{n+1})$ ▷ (6.14)

 Calculate S_{\max} ▷ (6.16)

 update β_n ▷ (6.19)

 Calculate $d_\tau \tilde{P}_n$ for ϕ^n ▷ (6.18)

 Solve $\underline{\underline{\mathbf{T}}}\Phi^{n+1} = \mathbf{Y}$ for Φ^{n+1} with $d_\tau \tilde{P}_n$ ▷ IMEX and FEM (5.14)

 Ensure $\|\phi^{n+1}\| \leq 1$ ▷ (5.21)

 Check path connectedness ▷ Algorithm 2

end while

end for

return ϕ^n

Plot results

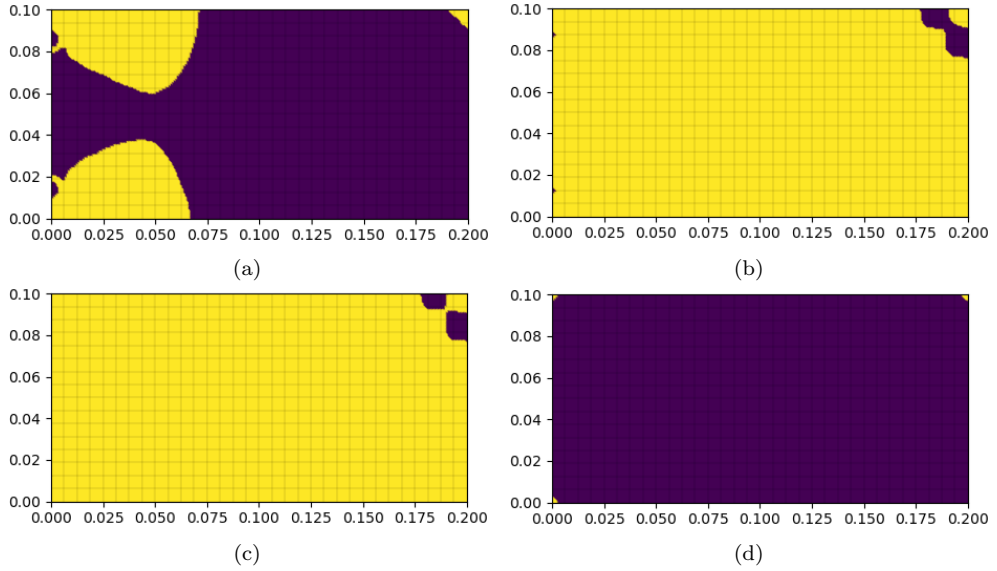


Figure 6.9: *Progress of Algorithm 3 for the 32 by 16 inverter: (a) material removal; (b) material introduction; (c) path connectedness; (d) everything removed.*

strain energy in the ersatz material becomes

$$S_{\max}(\phi^n, \phi^j) = \min \left\{ \frac{\tilde{S}(\phi^j) + \tilde{S}(\phi^n)}{2}, S_{\max}(\phi^n, \phi^{j-1}) \right\}. \quad (6.21)$$

Remark that Definition (6.21) enables us to use the strain energy in the ersatz material from before the breakup and from the newest level-set function. Moreover, it always uses the lowest value.

Algorithm 4 shows the pseudo-code of the alternative restoration algorithm.

It is, nonetheless, fairly unlikely that this algorithm will solve the issue. There is still no mechanical reason to connect the top right corner point to the rest of the structure. Presumably, Algorithm 4 will restore the connectivity after a number of iterations, but then the structure will break again. It will most likely not converge to an optimal design.

Algorithm 4 Alternative algorithm for minimum compliance with detection and restoration

Require: set input values

Initialise LSF

$S_{\max} = \infty$

$\beta = 0$

for $n \leftarrow 1$ to n_{\max} **do**

Solve $\tilde{a}_{\text{ext}}(\mathbf{u}, \mathbf{v}, \phi^n) = l(\mathbf{v})$ for \mathbf{u} ▷ FEM (5.17)

Calculate $\tilde{a}(\mathbf{u}, \mathbf{u}, \phi^n)$ ▷ FEM (4.24)

Calculate $\tilde{V}(\phi^n)$ ▷ (4.18)

if Optimisation criteria reached **then** ▷ Criteria: $\tilde{a}(\mathbf{u}, \mathbf{u}, \phi^n)$ and $\tilde{V}(\phi^n)$

 END for loop

end if

Update $d_\tau \tilde{P}_n$ for ϕ^j without γ_j ▷ (6.18)

Update γ_n ▷ Augmented Lagrange Method (6.20)

Solve $\underline{\mathbf{T}}\Phi^{n+1} = \mathbf{Y}$ for Φ^{n+1} with $d_\tau \tilde{P}_n$ ▷ IMEX and FEM (5.14)

Ensure $\|\phi^{n+1}\| \leq 1$ ▷ (5.21)

Check path connectedness ▷ Algorithm 2

if path connectedness is false **then**

 Calculate $S_{\max}(\phi^{\text{break}}, \phi^{n+1})$, last path connected LSF: ϕ^{path} ▷ (6.21)

 Update β_{n+1} ▷ (6.19)

if $\beta_{n+1} == 0$ **then**

$S_{\max} = \infty$

end if

end if

end for

return ϕ^n

Plot results

CHAPTER 7

CONCLUSION AND DISCUSSION

This is the final chapter of this thesis. First, we look at what has been achieved and from there we draw our conclusions. Finally, we discuss the used methods and propose ideas for further research.

7.1 Conclusion

In Chapter 2 a clear and generic framework was defined. This makes the methods we use more adaptable to tackle other problems besides the ones studied in this thesis. A mathematical derivation of the minimum compliance problem with a focus on the physics of linear elasticity was provided in Chapter 4. Such a derivation is quite scarce in literature and helps to understand the physics of the topology optimisation problems. When we solved the minimum compliance problem numerically, we pondered the available methods and justified the choice for our approach. Moreover, a clear and thorough description of the steps we took to solve the minimum compliance problem was given as well. In the papers mentioned in this thesis such thoroughness was mostly absent. To keep our initial design as simple as possible, we chose to have material everywhere in our reference frame. Unlike many other topology optimisation methods this initial design does not need any predefined holes for the final design to have holes as well. The obtained final designs have holes, because we incorporated the topological derivative into the update procedure of the level-set function. The results of the implementation of the level-set function are exceptional in comparison to the results of the comparative SIMP algorithm. The boundaries are very smooth as expected, even for a low number of elements. Furthermore, the structures seem to converge to a certain optimal structure, because the final designs look quite similar for a higher number of elements. This suggest, but does certainly not prove, that this level-set approach might not be mesh-dependent. Thus, looking at the final designs, we can conclude that the level-set approach provides results which have a smoother boundary and clearer distinction between the void and the material than the results of the SIMP approach. Moreover, the level-set approach does not rely on any kind of

filter to avoid the formation checkerboard.

In all final designs of the inverter (bottom half) a discontinuity occurred, which could have been anticipated, because we knowingly altered the objective of the original compliant inverter problem. Due to this change in objective, there was actually no mechanical reason to have material in the top right corner. There are two mechanical reasons to have material a priori in a point. There either is a force exerted on this point or it is fixed. In topology optimisation such points are automatically connected by optimisation algorithms, because there is a mechanical reason to connect them. As such a mechanical reason did not exist for the top right corner point in the inverter, this point was not connected to the main structure. Simply placing material in that point a priori and trying to pose a connectivity constraint did and will not change this, because the proposed algorithms do not have specific information regarding which points should be connected.

Unfortunately the author did not have this insight immediately and explored the possibilities to prevent such a discontinuity. We defined path connectedness and posed it as a constraint of the minimum compliance problem. To begin with, we developed an algorithm to check the path connectedness based on the nodal level-set values and the topology of the elements. Later, we devised a method which should restore path connectedness, if the structure broke during the optimisation process. Unfortunately this method did not work, looking at the results it delivered. So, an alternative restoration algorithm was provided, but not tested.

7.2 Discussion

Changing the original inverter problem from an optimum design problem of compliant mechanisms to a minimum compliance problem, heavily influenced the final design. Now, we do not know if the discontinuity in the minimum compliance problem would be present in the optimum design problem of compliant mechanisms. So, it would be interesting to investigate other problem objectives such as maximising the displacement in a single point, maximising the fundamental eigenfrequency or maximising the eigenfrequency gap to see if such discontinuities are commonplace. In addition to this, other benchmark problems would be interesting as well. In this thesis only one non-standard benchmark was tested. It would be more academic if more difficult benchmark problems are treated. Especially Michell structures [20] are interesting regarding the detection algorithm, as these structures have multiple force loads.

Looking at the results of the final designs with the level-set approach, we saw that the compliance increased during the optimisation process, contrary to the SIMP approach. This could be caused by the diffusive term in the reaction-diffusion equation as mentioned before, but it is more likely that it is caused by the removal of material to reach the volume constraint. If material is removed, there is less material to absorb the strain energy, so it rises substantially. A way to research this is to let the initial design be a slightly thinner version of the optimal design. Then, the optimisation algorithm should add material and lower the compliance. Parallel to this, the significance of the constant α could be inspected.

A huge drawback of the used code is how it handles the equation of motion, and makes

rounding errors when converting nodal values to elemental values and vice versa. The true essence of the level-set function is not used in the equation of motion, as the integration is performed over a 0-1 element-wise level-set function. The first problem could be circumvented with mesh fitting and refinement, in which case elements near the zero level-set curve would be refined and their edges placed on that curve. This creates a clear difference between material elements and void elements. This could, however, take a lot of CPU time and is quite difficult to implement. For the second problem no solution comes to mind, but this problem is negligible for fine meshes. Then, there is the introduction of ersatz material in the void. This, of course, also results in small errors in the final design, as it still influences the equation of motion. Ersatz material was introduced to prevent the global stiffness matrix of the equation of motion from becoming singular. This happens because we integrate over the entire reference frame. Again mesh fitting is the solution. This makes integrating over the entire reference frame redundant, as we know which elements approximate the material domain. So, we only have to integrate over those elements. A drawback is that the prevention algorithm, which relies on the strain energy in the ersatz material, cannot be used anymore.

The role of the Lagrangian γ should also be further explored. It seems to affect the volume constraint in an undesirable way. That is, the volume fraction does not converge to V_{\max} as we should expect, but often goes below that value. Although the volume constraint does allow this, it is logical to have as much material as possible, because that would make the structure more stiff.

It is obvious that the prevention algorithm should be analysed and tested further than is done in this thesis. The algorithm does not work and the suggested alternative restoration algorithm is not yet tested. Maybe the current approach with a focus on the ersatz material is not the best and other possibilities, such as the extended finite-element method (XFEM), should be considered.

The algorithm to detect path connectedness is adequate, but fairly slow in terms of CPU time. It would be compelling to develop a similar detection algorithm based on the edges and nodes, instead of the elements and nodes. This would make way for the implementation of Dijkstra's algorithm (named after Edsger Dijkstra).

A particularly ambitious study would be tackling three dimensional benchmark problems. This thesis merely provides the generic models which could be used for three dimensional objects as well, but solely treats two dimensional benchmarks. Note that a completely different detection algorithm has to be devised in the three dimensional case, as the topology of the elements changes.

Finally, there is definitely more research needed to determine if the level-set approach is better than the SIMP approach or any other approach for that matter. The results of this thesis are promising and in favour of the level-set approach, but more tests are essential to be conclusive.

APPENDIX A

DERIVATION OF THE EQUATION OF MOTION

To derive the equilibrium equation of motion for linear elasticity, we have to alter the right hand side of Equation (4.11).

$$\begin{aligned}
 \underline{\underline{\sigma}} : \underline{\underline{\varepsilon}}(\mathbf{v}) &= \underline{\underline{\sigma}} : \left[\frac{1}{2} (\nabla \mathbf{v} + (\nabla \mathbf{v})^T) \right] \\
 &= \frac{1}{2} [\underline{\underline{\sigma}} : \nabla(\mathbf{v})] + \frac{1}{2} [\underline{\underline{\sigma}} : (\nabla \mathbf{v})^T] \\
 &= \frac{1}{2} [\underline{\underline{\sigma}} : \nabla(\mathbf{v})] + \frac{1}{2} [\underline{\underline{\sigma}}^T : (\nabla \mathbf{v})^T] \\
 &= \frac{1}{2} [\underline{\underline{\sigma}} : \nabla(\mathbf{v})] + \frac{1}{2} [\underline{\underline{\sigma}} : \nabla \mathbf{v}] = \underline{\underline{\sigma}} : \nabla(\mathbf{v}).
 \end{aligned}$$

So we have

$$\underline{\underline{\sigma}} : \underline{\underline{\varepsilon}}(\mathbf{v}) = \underline{\underline{\sigma}} : \nabla(\mathbf{v}).$$

Now Equation (4.11) becomes

$$\int_{\Omega} \underline{\underline{\sigma}}(\mathbf{u}) : \nabla \mathbf{v} \, d\Omega = \int_{\Omega} \mathbf{f} \cdot \mathbf{v} \, d\Omega + \int_{\Gamma} \mathbf{t} \cdot \mathbf{v} \, d\Gamma. \quad (\text{A.1})$$

We introduce the *traction-stress relation* [37] for all \mathbf{u} on the boundary Γ_N :

$$\mathbf{t} = \hat{\mathbf{n}} \cdot \underline{\underline{\sigma}}(\mathbf{u}), \quad t_i = \hat{n}_j \sigma_{ji}(\mathbf{u}), \quad (\text{A.2})$$

where $\hat{\mathbf{n}}$ is the unit normal vector. This gives

$$\mathbf{t} \cdot \mathbf{v} = (\hat{\mathbf{n}} \cdot \underline{\underline{\sigma}}(\mathbf{u})) \cdot \mathbf{v} = \underline{\underline{\sigma}}^T(\mathbf{u}) \hat{\mathbf{n}} \cdot \mathbf{v} = \underline{\underline{\sigma}}(\mathbf{u}) \mathbf{v} \cdot \hat{\mathbf{n}}.$$

We substitute this into Equation (A.1) and bring the boundary integral to the left hand side.

$$\int_{\Omega} \underline{\underline{\sigma}}(\mathbf{u}) : \nabla \mathbf{v} \, d\Omega - \int_{\Gamma} \underline{\underline{\sigma}}(\mathbf{u}) \mathbf{v} \cdot \hat{\mathbf{n}} \, d\Gamma = \int_{\Omega} \mathbf{f} \cdot \mathbf{v} \, d\Omega. \quad (\text{A.3})$$

Now we apply Gauß' divergence theorem [38].

$$\int_{\Omega} \underline{\underline{\sigma}}(\mathbf{u}) : \nabla \mathbf{v} \, d\Omega - \int_{\Omega} \nabla \cdot (\underline{\underline{\sigma}}(\mathbf{u}) \mathbf{v}) \, d\Omega = \int_{\Omega} \mathbf{f} \cdot \mathbf{v} \, d\Omega$$

We take a look at the integrand of the second integral on the left hand side and work it out.

$$\begin{aligned} \nabla \cdot (\underline{\underline{\sigma}} \mathbf{v}) &= \sum_{i,j=1}^d \frac{\partial}{\partial x_i} (\sigma_{ij} v_j) \\ &= \sum_{i,j=1}^d v_j \frac{\partial \sigma_{ij}}{\partial x_i} + \sum_{i,j=1}^d \sigma_{ji} \frac{\partial v_i}{\partial x_j} \\ &= (\nabla \cdot \underline{\underline{\sigma}}^T) \cdot \mathbf{v} + \underline{\underline{\sigma}}^T : \nabla \mathbf{v} = (\nabla \cdot \underline{\underline{\sigma}}) \cdot \mathbf{v} + \underline{\underline{\sigma}} : \nabla \mathbf{v} \end{aligned}$$

This gives the weak form of the equilibrium equation

$$\int_{\Omega} [\nabla \cdot \underline{\underline{\sigma}}(\mathbf{u}) + \mathbf{f}] \cdot \mathbf{v} \, d\Omega = 0. \quad (\text{A.4})$$

From the Du Bois-Reymond lemma (named after Paul du Bois-Reymond and also know as the Fundamental Lemma of the calculus of variations see [26]) it follows that

$$-\nabla \cdot \underline{\underline{\sigma}}^T(\mathbf{u}) = \mathbf{f}, \quad -\sigma_{ji,j} = f_i. \quad (\text{A.5})$$

Now, together with the traction-stress relation (A.2) and boundary conditions we find that the displacement \mathbf{u} in the field D is the solution of the following boundary value problem:

$$\begin{cases} -\nabla \cdot \underline{\underline{\sigma}}^T(\mathbf{u}) = \mathbf{f}, & \forall \mathbf{u} \in D, \\ \mathbf{u} = \mathbf{u}_0 & \forall \mathbf{u} \in \Gamma_D, \\ \hat{\mathbf{n}} \cdot \underline{\underline{\sigma}}(\mathbf{u}) = \mathbf{t}, & \forall \mathbf{u} \in \Gamma_N. \end{cases} \quad (\text{A.6})$$

APPENDIX B

NOMENCLATURE

Notation	Definition	SI unit
ρ	Density	$\text{kg}\cdot\text{m}^{-3}$
\mathbf{x}	Place vector	m
\mathbf{u}	Displacement vector	m
$\underline{\underline{\varepsilon}}$	Strain-displacement tensor	-
$\underline{\underline{\sigma}}$	Stress tensor	Pa
E	Young's modulus	Pa
ν	Poisson ratio	-
λ	Lamé's first constant	Pa
μ	Lamé's second constant	Pa
E_{ijkl}	Stiffness tensor element	Pa

BIBLIOGRAPHY

- [1] G. Allaire. The Homogenization Method for Topology and Shape Optimization. *Topology Optimization in Structural Mechanics*, 374:101–133, 1997. doi: 10.1007/978-3-7091-2566-3_3.
- [2] G. Allaire and F. Jouve. A level-set method for vibration and multiple loads structural optimization. *Computer Methods in Applied Mechanics and Engineering*, 194(30-33 SPEC. ISS.):3269–3290, 2005. ISSN 00457825. doi: 10.1016/j.cma.2004.12.018.
- [3] G. Allaire and F. Jouve. Minimum stress optimal design with the level set method. *Engineering Analysis with Boundary Elements*, 32(11):909–918, 2008. ISSN 09557997. doi: 10.1016/j.enganabound.2007.05.007.
- [4] G. Allaire, F. Jouve, and A. M. Toader. A level-set method for shape optimization. *Comptes Rendus Mathematique*, 334(12):1125–1130, 2002. ISSN 1631073X. doi: 10.1016/S1631-073X(02)02412-3.
- [5] G. Allaire, F. Jouve, and A. M. Toader. *Structural optimization using sensitivity analysis and a level-set method*, volume 194. 2004. ISBN 3316933301. doi: 10.1016/j.jcp.2003.09.032.
- [6] G. Allaire, F. De Gournay, F. Jouve, and A. M. Toader. Structural optimization using topological and shape sensitivity via a level set method. *Control and Cybernetics*, 34(1):59–81, 2005. ISSN 03248569.
- [7] S. S. Antman. *Nonlinear Problems of Elasticity*. Springer, New York, second edition, 2005. ISBN 978-0-387-20880-0. doi: <https://doi-org.tudelft.idm.oclc.org/10.1007/0-387-27649-1>.
- [8] M. P. Bendsøe and N. Kikuchi. Generating optimal topologies in structural design using a homogenization method. *Computer Methods in Applied Mechanics and Engineering*, 71(2):197–224, 1988. doi: 10.1016/0045-7825(88)90086-2.

-
- [9] M.P. Bendsøe and O. Sigmund. *Topology optimization: Theory, Methods and Applications*. 2003. ISBN 3540429921. doi: 10.1007/978-3-7091-1309-7_3.
- [10] S. Boyd and L. Vandenberghe. *Convex Optimization*. Cambridge University Press, 1 edition, 2004. ISBN 0521833787. doi: 10.1201/9781315366920-5.
- [11] F. De Gournay. Velocity extension for the level-set method and multiple eigenvalues in shape optimization. *SIAM Journal on Control and Optimization*, 45(1):343–367, 2006. ISSN 03630129. doi: 10.1137/050624108.
- [12] J. D. Deaton and R. V. Grandhi. A survey of structural and multidisciplinary continuum topology optimization: Post 2000. *Structural and Multidisciplinary Optimization*, 49(1):1–38, 2014. ISSN 1615147X. doi: 10.1007/s00158-013-0956-z.
- [13] V. A. Eremeyev and L. P. Lebedev. Existence of weak solutions in elasticity. *Mathematics and Mechanics of Solids*, 18(2):204–217, 2013. ISSN 10812865. doi: 10.1177/1081286512462187.
- [14] A. L. Gain and G. H. Paulino. A critical comparative assessment of differential equation-driven methods for structural topology optimization. *Structural and Multidisciplinary Optimization*, 48(4):685–710, 2013. ISSN 16151488. doi: 10.1007/s00158-013-0935-4.
- [15] I. Gibson, D. W. Rosen, B. Stucker, and M. Khorasani. *Additive Manufacturing Technologies*. Springer, Cham, 3 edition, 2021. ISBN 9783030561277. doi: 10.1007/978-3-030-56127-7.
- [16] A. Kasaiezadeh and A. Khajepour. Application of level set method to the design of mechanical components with a desired multi-dimensional stiffness. *Vehicle System Dynamics*, 49(1-2):75–86, 2011. ISSN 00423114. doi: 10.1080/00423110903401897.
- [17] T. Lewiński, M. Zhou, and G. I. N. Rozvany. Extended exact least-weight truss layouts-Part II: Unsymmetric cantilevers. *International Journal of Mechanical Sciences*, 36(5):399–419, 1994. ISSN 00207403. doi: 10.1016/0020-7403(94)90044-2.
- [18] T. Lewiński, M. Zhou, and G. I. N. Rozvany. Extended exact solutions for least-weight truss layouts-Part I: Cantilever with a horizontal axis of symmetry. *International Journal of Mechanical Sciences*, 36(5):375–398, 1994. ISSN 00207403. doi: 10.1016/0020-7403(94)90043-4.
- [19] T. Lewiński, G. I. N. Rozvany, T. Sokół, and K. Bołbotowski. Exact analytical solutions for some popular benchmark problems in topology optimization III: L-shaped domains revisited. *Structural and Multidisciplinary Optimization*, 47(6):937–942, 2013. ISSN 1615147X. doi: 10.1007/s00158-012-0865-6.
- [20] A. G. M. Michell. The limits of economy of material in frame-structures. *The London, Edinburgh, and Dublin Philosophical Magazine and Journal of Science*, 8(47):589–597, 1904. ISSN 1941-5982. doi: 10.1080/14786440409463229.

-
- [21] L. Noël, M. Schmidt, C. Messe, J. A. Evans, and K. Maute. Adaptive level set topology optimization using hierarchical B-splines. *Structural and Multidisciplinary Optimization*, 62(4):1669–1699, 2020. doi: 10.1007/s00158-020-02584-6.
- [22] A. A. Novotny and J. Sokołowski. *Topological derivatives in shape optimization*. Springer, 2013. ISBN 9783642352454. doi: 10.1007/978-3-642-35245-4.
- [23] S. Osher and R. P. Fedkiw. *Level set methods and dynamic implicit surfaces*. Springer, New York, 2003. ISBN 9781468492514. doi: 10.1007/0-387-22746-6_2.
- [24] S. Osher and J. A. Sethian. Fronts propagating with curvature dependent speed: algorithms based on Hamilton-Jacobi formulations. *Journal of Computational Physics*, 148(1):12–49, 1988.
- [25] M. Otomori, T. Yamada, K. Izui, and S. Nishiwaki. Matlab code for a level set-based topology optimization method using a reaction diffusion equation. *Structural and Multidisciplinary Optimization*, 51(5):1159–1172, 2015. ISSN 16151488. doi: 10.1007/s00158-014-1190-z.
- [26] F. Rindler. *Calculus of variations*. Springer, 2018. ISBN 9783319776378. doi: 10.1007/978-3-319-77637-8.
- [27] G. I. N. Rozvany. Analytical benchmarks in topology optimization - Including probabilistic design. *12th AIAA/ISSMO Multidisciplinary Analysis and Optimization Conference, MAO*, (September):1–11, 2008. doi: 10.2514/6.2008-5941.
- [28] G. I. N. Rozvany. On symmetry and non-uniqueness in exact topology optimization. *Structural and Multidisciplinary Optimization*, 43(3):297–317, 2011. ISSN 1615147X. doi: 10.1007/s00158-010-0564-0.
- [29] J. J. Rushchitsky. *Nonlinear elastic waves in materials*. Springer, 2014. ISBN 9783319004631. doi: 10.1007/978-3-319-00464-8.
- [30] M. H. Sadd. *Elasticity: Theory, applications, and numerics, third edition*. 2014. ISBN 9780124081369. doi: 10.1016/B978-0-12-408136-9.01001-1.
- [31] J. A. Sethian and A. Wiegmann. Structural Boundary Design via Level Set and Immersed Interface Methods. *Journal of Computational Physics*, 163(2):489–528, 2000. ISSN 00219991. doi: 10.1006/jcph.2000.6581.
- [32] O. Sigmund. On the design of compliant mechanisms using topology optimization. *Mechanics of Structures and Machines*, 25(4):493–524, 1997. ISSN 08905452. doi: 10.1080/08905459708945415.
- [33] O. Sigmund. Morphology-based black and white filters for topology optimization. *Structural and Multidisciplinary Optimization*, 33(4-5):401–424, 2007. ISSN 1615147X. doi: 10.1007/s00158-006-0087-x.
- [34] O. Sigmund. Manufacturing tolerant topology optimization. *Acta Mechanica Sinica*, 25(2):227–239, 2009. ISSN 05677718. doi: 10.1007/s10409-009-0240-z.

- [35] O. Sigmund and K. Maute. Topology optimization approaches: A comparative review. *Structural and Multidisciplinary Optimization*, 48(6):1031–1055, 2013. ISSN 1615147X. doi: 10.1007/s00158-013-0978-6.
- [36] O. Sigmund and J. Petersson. Numerical instabilities in topology optimization: A survey on procedures dealing with checkerboards, mesh-dependencies and local minima. *Structural Optimization*, 16(1):68–75, 1998. ISSN 09344373. doi: 10.1007/BF01214002.
- [37] W. S. Slaughter and J. Petrolito. *The Linearized Theory of Elasticity*. Springer, 2002. ISBN 9781461266082. doi: 10.1115/1.1497478.
- [38] M. R. Spiegel. *Vector Analysis*. Schaum;s Outlines, 2010. doi: 10.1119/1.1933387.
- [39] K Suzuki and N Kikuchi. A homogenization method for shape and topology optimization. *Computer Methods in Applied Mechanics and Engineering*, 93(3): 291–318, 1991. ISSN 01608835. doi: 10.1016/0045-7825(91)90245-2.
- [40] K. Svanberg. The method of moving asymptotes - a new method for structural optimisation. 24(June 1986):359–373, 1987.
- [41] A. Takezawa, S. Nishiwaki, and M. Kitamura. Shape and topology optimization based on the phase field method and sensitivity analysis. *Journal of Computational Physics*, 229(7):2697–2718, 2010. ISSN 10902716. doi: 10.1016/j.jcp.2009.12.017. URL <http://dx.doi.org/10.1016/j.jcp.2009.12.017>.
- [42] N. P. Van Dijk, K. Maute, M. Langelaar, and F. Van Keulen. Level-set methods for structural topology optimization: A review. *Structural and Multidisciplinary Optimization*, 48(3):437–472, 2013. ISSN 16151488. doi: 10.1007/s00158-013-0912-y.
- [43] E. Vegería, R. Ansola, A. Maturana, and J. Canales. Topology synthesis of compliant mechanisms using an evolutionary method. In *International Conference on Engineering Optimization*, 2008.
- [44] F. Vermolen, J. van Kan, and A. Segal. *Numerical Methods in Scientific Computing*. Delft Academic Press, Delft, 2 edition, 2014. ISBN 9789065623638.
- [45] K. Yaji, M. Otomori, T. Yamada, K. Izui, S. Nishiwaki, and O. Pironneau. Shape and topology optimization based on the convected level set method. *Structural and Multidisciplinary Optimization*, 54(3):659–672, 2016. ISSN 16151488. doi: 10.1007/s00158-016-1444-z. URL <http://dx.doi.org/10.1007/s00158-016-1444-z>.
- [46] T. Yamada, K. Izui, S. Nishiwaki, and A. Takezawa. A topology optimization method based on the level set method incorporating a fictitious interface energy. *Computer Methods in Applied Mechanics and Engineering*, 199(45):2876–2891, 2010. ISSN 00457825. doi: 10.1016/j.cma.2010.05.013. URL <http://dx.doi.org/10.1016/j.cma.2010.05.013>.
- [47] D. Zwillinger. *CRC Standard Mathematical Tables and Formulae*. CRC Press LLC, 31 edition, 2003. ISBN 9781439835487.